Supplementary Material for

Pulmonary surfactant–biomimetic nanoparticles potentiate heterosubtypic influenza immunity

Ji Wang, Peiyu Li, Yang Yu, Yuhong Fu, Hongye Jiang, Min Lu, Zhiping Sun, Shibo Jiang, Lu Lu*, Mei X. Wu*

*Corresponding author. Email: mwu5@mgh.harvard.edu (M.X.W.); lul@fudan.edu.cn (L.L.)

Published 21 February 2020, *Science* **367**, eaau0810 (2020)
DOI: 10.1126/science.aau0810

This PDF file includes:

Extended Materials and Methods

Hemagglutination inhibition (HAI) assays

Serum samples were collected at indicated times from immunized and control animals and treated with receptor-destroying enzyme (RDE) (Denka Seiken, Tokyo, Japan) at 37°C for 20 hrs followed by heat inactivation at 56°C for 30 min. The resultant serum samples were serially diluted and incubated with 4 hemagglutination units (HAU) of an indicated influenza virus at 37°C for 1 h. The serum-treated virus was incubated with 0.5% chicken red blood cells (for H1N1 and H7N9) or horse red blood cells (for H5N1) at room temperature for 30 minutes. The HAI titer was defined as the reciprocal of the highest serum dilution that inhibited 4 HAU of a given virus.

Enzyme-linked immunosorbent assay (ELISA)

Influenza-specific IgG, IgG1, IgG2a, IgA, IgM, and IgG2c antibody titers were measured by ELISA. In brief, 1 μg/ml of recombinant HA was coated onto ELISA plates in $NaHCO_3$ buffer, pH 9.6 overnight, to which serially diluted serum samples were added. Antibody subtypes were quantified by HRP-conjugated goat anti-mouse IgG (NA931V, GE healthcare, dilution 1:6000), IgG1 (1073-05, Southern Biotech, 1:4000), IgG2c (1079-05, Southern Biotech, 1:4000), IgA (A90-103P, Bethyl, 1:10000), IgM (ab97230, 1:20000) or IgG2a (1083-05, Southern Biotech, 1:4000) antibody. Titers of specific antibody subtypes were quantified by using SIGMAFAS^{TM} OPD as the substrate and reading the reaction at A490 on a plate reader (Molecular Devices).

Cellular immune responses

Splenocytes were isolated from mice 7 d post-immunization by passing the spleens through 40-μm strainers, followed by lysis of red blood cells with ACK (Ammonium-Chloride-Potassium) buffer for 4 min on ice. Cells at 1×10^6/ml were incubated with influenza vaccine (1 μg/ml) and 4 μg/ml of anti-CD28 (clone 37.51, BD Pharmingen) antibody overnight. Golgi-Plug (BD Pharmingen) was added to the culture and incubated for another 5 h. The stimulated cells were first stained with fluorescence-conjugated antibodies against CD3, CD4, and CD8, followed by intracellular staining with anti-IFN-γ antibody. All antibodies were listed in Table S2. The stained cells were acquired on a FACSAria II (BD) and analyzed using FlowJo software (Tree Star).

Chimeric mice generated by bone marrow transplantation

Chimeric mice were generated by bone marrow (BM) transplantation as described (*33*). Briefly, BM cells were harvested from femur and tibia of gender- and age-matched donor mice different in CD45 alleles. Recipient mice received lethal irradiation from ^{137}Cs gamma irradiator (Mark I, 30 J.L. Shepherd) at a dose of 1100 rad administered in two fractions at 3 h apart. Right after the second irradiation, 5×10^6 donor BM cells were intravenously injected into recipient mice. BM cells of STING-deficient mice (*Sting*$^{-/-}$ or ST) were transferred to age and gender-matched WT mice or vice versa. WT mice receiving WT BM cells or ST mice receiving ST BM cells were also prepared in parallel. Mice were supplied with antibiotics-containing water from 5 d before irradiation to 14 d after irradiation and housed for 3 months to establish complete reconstitution of donor populations, which was corroborated by flow cytometric analysis of lungs, MLNs,

spleens, and peripheral blood mononuclear cells (PBMCs) after staining with anti-CD45.1 (clone A20, BioLegend, 2 μg/ml) or anti-CD45.2 (clone 104, BioLegend, 2.5 μg/ml) antibody.

BM-derived dendritic cells (BMDCs) and BM-derived macrophages (BMMs)

BMDCs and BMMs were prepared as previously described (*45*). Briefly, BM cells were harvested from tibiae and femurs of 4-6-week-old C57BL/6 mice. Cells at a concentration of 1×10^6 / ml were cultured with 10 ng/ml granulocyte macrophage colony stimulating factor (GM-CSF) or 100 ng/ml macrophage colony stimulating factor (M-CSF) for 7 days to generate BMDCs or BMMs, respectively. $CD11c^+$ BMDCs were further purified by high-speed cell sorting in FACSAria II (BD).

Requirement of PS for AM uptake of nano4 in non-human primates (NHP)

Lungs were surgically removed after rhesus macaques were euthanized, filled with 150 ml of cold RPMI 1640 medium supplemented with antibiotics, immersed in the cold medium, and transported to the laboratory on ice. The AMs and PS were isolated as described (*46*). Briefly, the filled RPMI 1640 medium was collected from the lung and centrifuged at 200×*g* to remove cell debris and then at 8000×*g* for 20 min to pellet PS. The supernatant (30 ml) was concentrated to 1 ml by 10 kDa Amicon Ultra Centrifugal Filter Units (Merk Millipore) and mixed with PS pellet prepared above to obtain concentrated PS with both lipids and surfactant proteins. AMs were isolated by washing the lung six times with 100 ml of PBS containing 0.5 mM EDTA. The lung lavages were pooled and centrifuged at 200×*g* to collect the cells. The cells were washed thoroughly with PBS and cultured in RPMI 1640 for 20 min, followed by removal of nonadherent cells. The concentrated PS at 2 mg of total proteins was mixed with DiD-nano4 or DiD-nano5 (48 μg lipid content) for 30 min and then incubated with 1.6×10^5 AMs in 1 ml of medium for 3 h at 37℃ with 5% CO_2. AMs were stained with a vital dye Calcein-AM (Life Technologies) and Hoechst (Sigma). AM uptake of the nanoparticles was evaluated by confocal microscopy (Olympus FV3000, UPLSAPO 40×) and analyzed by ImageJ software.

Transmission electron microscopy (TEM)

To determine ultrastructural localization of nano4 and nano5 in alveoli, nanogold (5 nm, Alfa Aesar) was encapsulated into nano4 or nano5 by reverse-phase evaporation as described (*47*). Mice were i.n. administered with nanogold-nano4 or nano5 at an equal amount, 12 h after which lungs were isolated, fixed in Karnovsky fixative at 4℃ overnight, post-fixed in 1% OsO4 in 0.1 M sodium cacodylate buffer for 1.5 h, dehydrated in gradient alcohol series, infiltrated with s-propylene oxide/Epon t812 gradient mixture, and embedded in Epon t812 (Tousimis). Ultrathin sections were cut at 80 nm on a microtome (Reichert-Jung Ultracut E), collected on 100-mesh copper grids, stained with 2% Uranyl Acetate and Lead Citrate (2.66% lead nitrate, 3.52% sodium citrate), and examined on a CM-10 transmission electron microscope (Philips). Digital TEM images were taken by AMT-XR41M 4.0 Megapixel Cooled sCMOS camera (Advanced Microscopy Techniques).

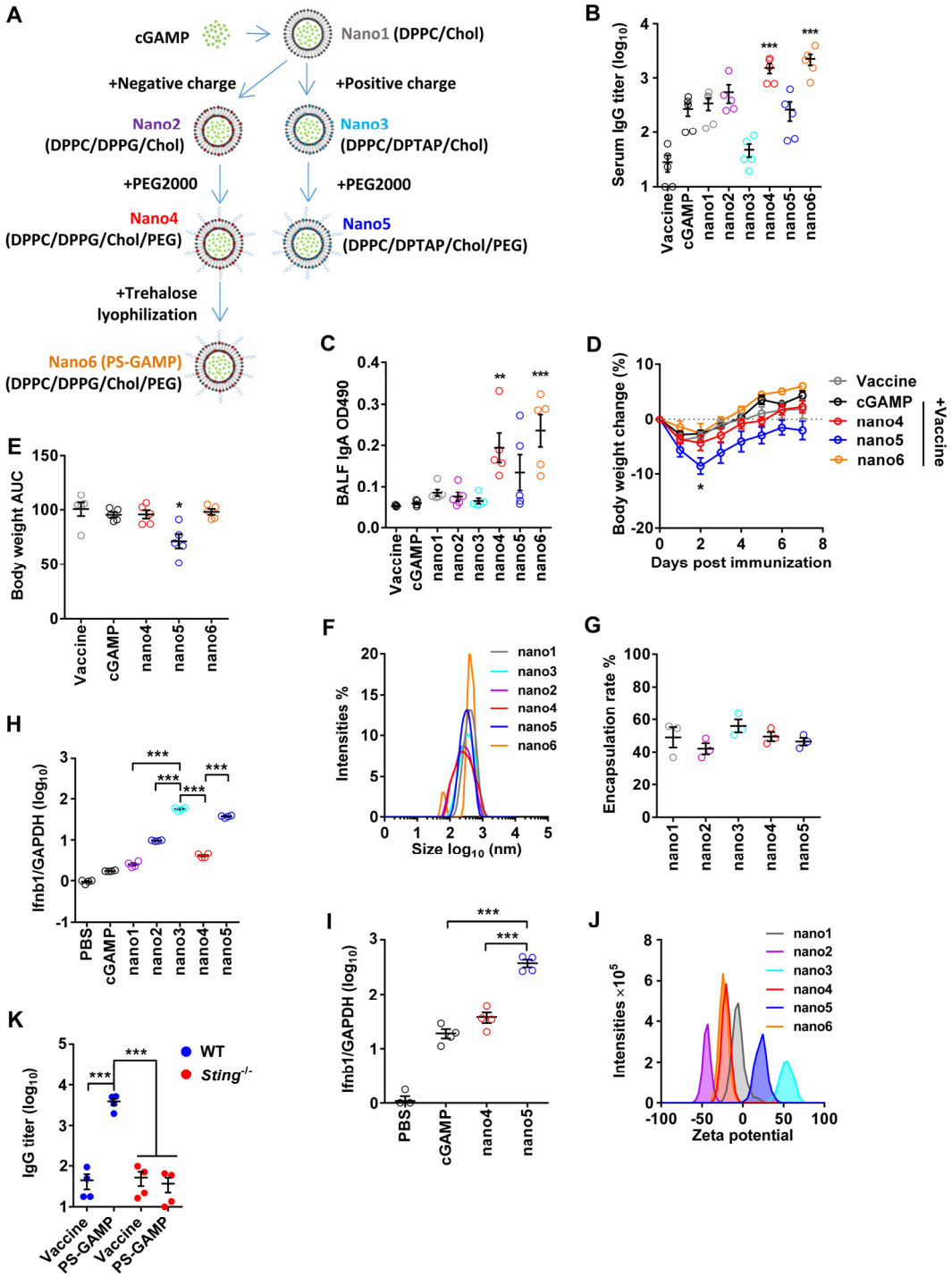

Fig. S1. PS-GAMP fabrication and characterization.

(**A**) A schematic diagram of PS-GAMP fabrication. The liposomes were synthesized in the basis of PS ingredients of mammals, which typically consists of 90% lipids and 10% proteins and is evolutionally conserved. The lipids contain 8-10% of cholesterol, 60-70%

of zwitterionic phosphatidylcholines (PC), mainly dipalmitoylated phosphatidylcholine (DPPC), up to 8-15% of anionic phosphatidylglycerol (DPPG), and a relatively small portion of other lipids (*17*). PEG2000 was utilized in place of hydrophilic proteins and DPPG was replaced with cationic DPTAP in nano3 and nano5 to determine the importance of charges. These PS lipids and PEG2000 form liposomes with a single lipid bilayer encapsulating cGAMP by reverse-phase evaporation as detailed in Materials and Methods. (**B** to **E**) Swiss Webster mice were i.n. immunized with VN04 H5N1 vaccine (1 μg HA content) plus 10 μg free cGAMP or an equal amount of cGAMP packaged in the indicated liposomes. Serum IgG (**B**) and bronchoalveolar lavage fluid (BALF) IgA (**C**) were measured two weeks later, body weight was monitored for 7 d after immunization (**D**) and the area under the curve (AUC) was calculated from (**D**) by PRISM software (**E**). n=5. Sizes (**F**), encapsulation rate (**G**), and zeta potentials (**J**) of indicated liposomes were measured. (**H** and **I**) Free cGAMP or cGAMP-encapsulated liposomes were cultured with BMDCs (**H**) and BMMs (**I**) at a final cGAMP concentration of 10 μg/ml for 8 h, after which IFN-β (*Ifnb1*) was measured by real-time RT-PCR. n=4. (**K**) STING-deficient mice (*Sting*$^{-/-}$) (**Red**) or wild-type (WT) (**Blue**) control mice were i.n. immunized with VN04 H5N1 vaccine alone or together with PS-GAMP and serum IgG titers were measured 2 weeks later as above. n=4. The results were presented as means ± SEM. Each symbol represents individual mice in (**B**, **C**, **E**, and **K**) or independent duplicates in (**G, H,** and **I**). Statistical analysis, one-way ANOVA for (**B, C, E,** and **H-K**), two-way ANOVA for (**D**). *p<0.05, **p<0.01, and ***p<0.001 compared to vaccine alone group or between indicated groups. All experiments were repeated twice with similar results.

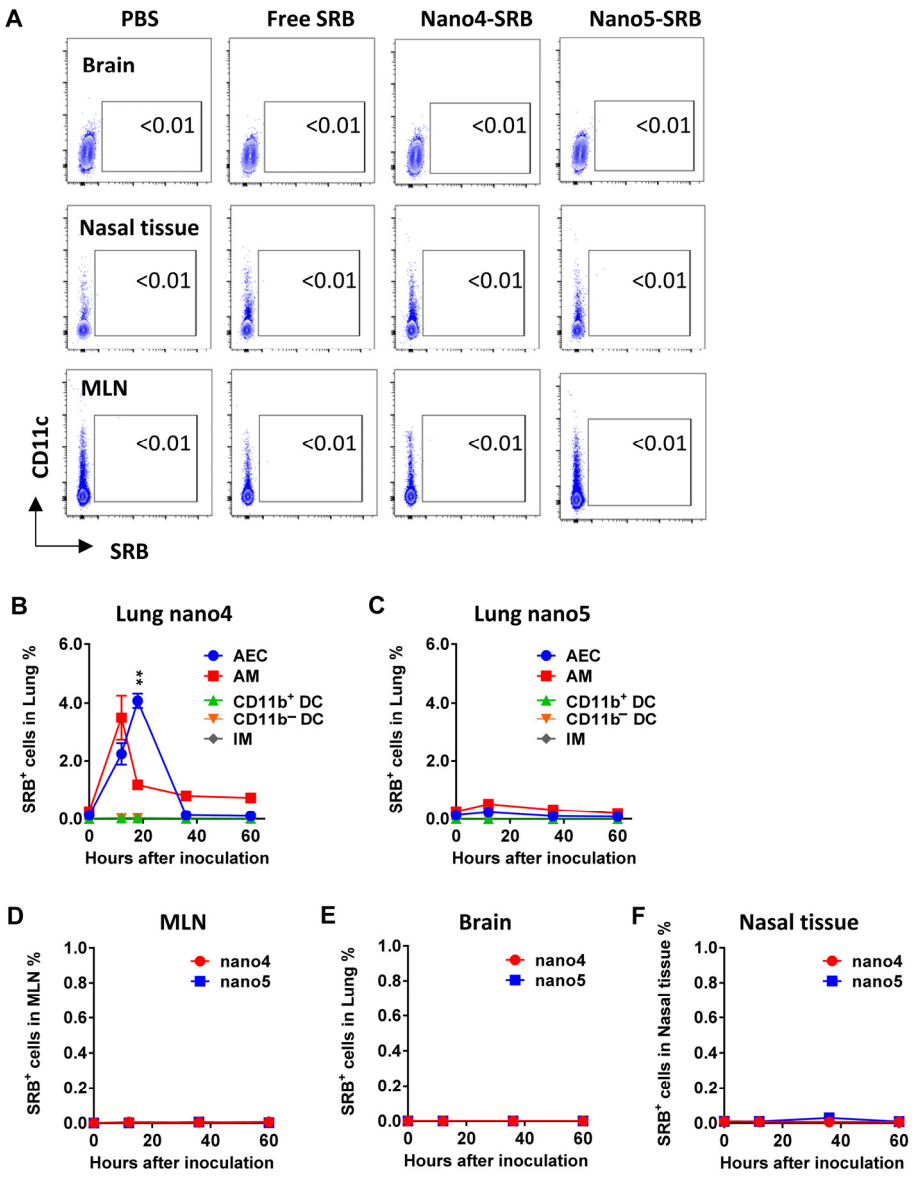

Fig. S2. Kinetics of nanoparticle uptake in different tissues.

Mice were i.n. administered PBS, free SRB, SRB-encapsulated and DiD-labeled nano4 (Nano4-SRB) or SRB-encapsulated and DiD-labeled nano5 (Nano5-SRB) and analyzed by flow cytometry at varying times. (**A**) Representative flow plots for SRB^+ cells in the brain (upper), nasal tissue (middle), and MLN (lower). Data are representative of two separate experiments each assayed in triplicate. (**B** and **C**) SRB^+ cells in the lungs of mice receiving nano4-SRB (**B**) or nano5-SRB (**C**). Alveolar macrophages (AM), interstitial macrophages (IM), $CD11b^+$DCs, and $CD11b^-$DCs were gated as **fig. S3**. (**D-F**) SRB^+ cells in MLN (**D**), brain (**E**), or nasal tissue (**F**) of mice receiving nano4-SRB or nano5-SRB. n=4. The results were presented as means ± SEM. Statistical analysis, two-way ANOVA for (**B-F**). *p<0.05, **p<0.01, and ***p<0.001. The experiment was repeated twice with similar results.

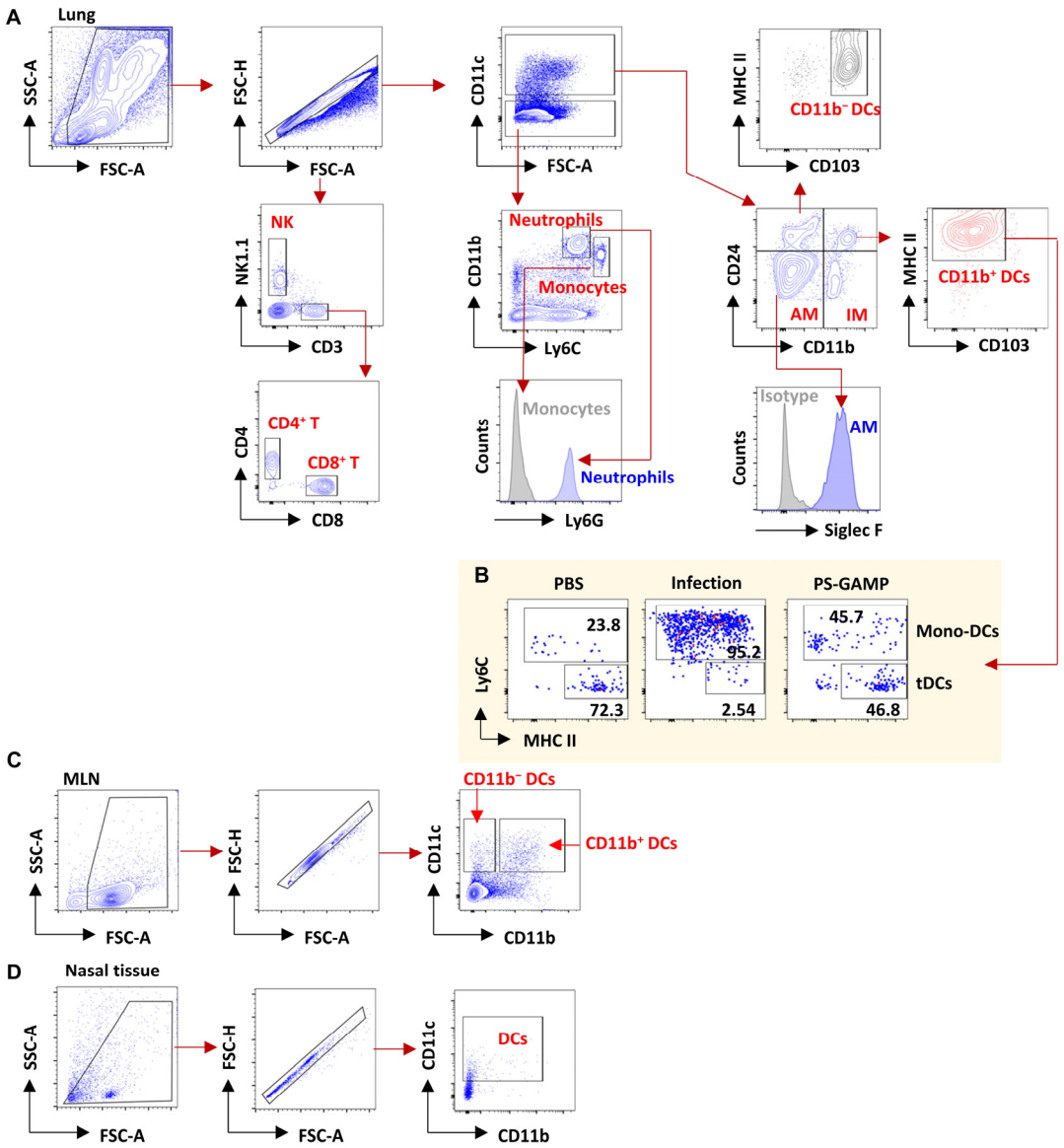

Fig. S3. Gating strategy for flow cytometric analysis of cells isolated from indicated tissues.

(**A**) NK cells were identified by NK1.1^{+} and CD3^{-} in pulmonary cells and CD3^{+} cells were separated into CD4^{+} and CD8^{+} T cells. Pulmonary CD11c^{-} cells were divided into neutrophils as CD11b^{+}Ly6C^{+}Ly6G^{+}, whereas inflammatory monocytes were recognized as CD11b^{+}Ly6C^{hi}Ly6G^{-}. On the gate of CD11c^{+} cells, four populations were discriminated with CD24 and CD11b markers, among which AMs were CD24^{-}CD11b^{-}Siglec F^{+}, IMs were CD24^{-}CD11b^{+}, CD24^{+}CD11b^{-}DCs were CD103^{+} MHC II^{+}, and tissue-resident CD24^{+}CD11b^{+} DCs also expressed MHC II but not CD103. (**B**) During influenza virus infection or after PS-GAMP administration, CD11b^{+} DCs could be separated into monocyte-derived DCs (Mono-DCs) or tissue resident-like DCs (tDCs). Mono-DCs were Ly6C^{hi} and MHC II expression varied with their activation

status. On the other hand, tDCs were Ly6C^{lo}MHC II^{hi}. (**C** and **D**) Gating strategy for CD11b^{+}DCs and CD11b^{-} DCs in MLN (**C**) or DCs in nasal tissue (**D**). Gating strategies for T cells, NK cells, neutrophils, and monocytes in MLN, nasal tissue, and brain were similar to those in the lung (**A**).

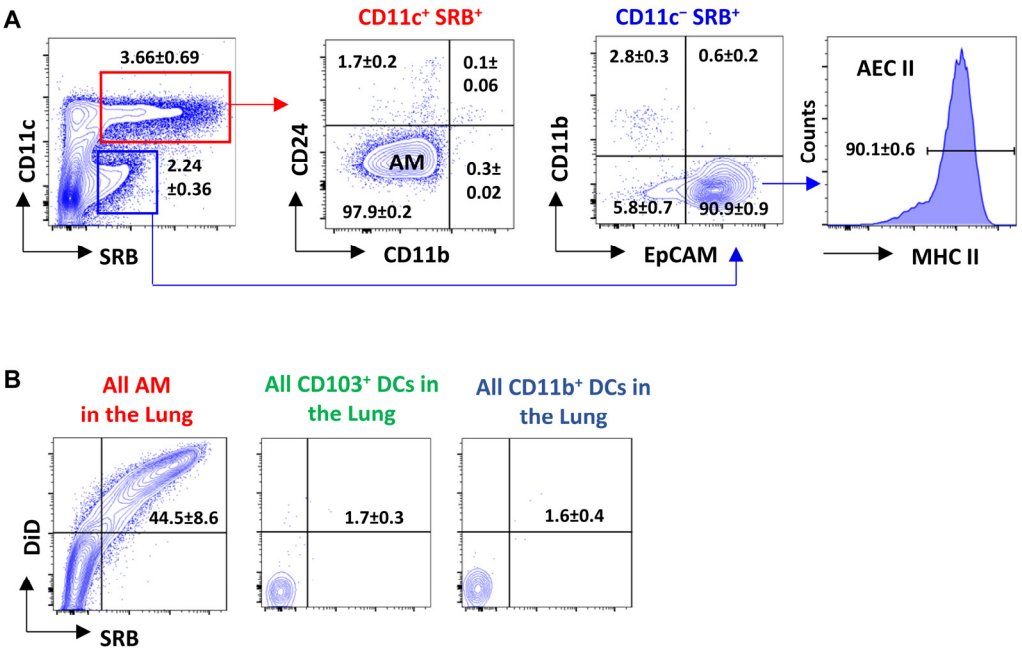

Fig. S4. Analysis of cells capturing PS-liposomes in the lung.

(**A**) Mice were i.n. administered nano4-SRB prepared as **Fig. 1A**. Twelve h later, $CD11c^{+}SRB^{+}$ cells were characterized mostly as $CD24^{-}CD11b^{-}$ AMs, and $CD11c^{-}SRB^{+}$ cells were mostly $EpCAM^{+}CD11b^{-}$ AECs, which were also positive for MHC II. (**B**) AMs, $CD103^{+}$ DCs, and $CD11b^{+}$ DCs gated as **fig. S3A** were analyzed for direct nanoparticle uptake ($SRB^{+}DiD^{+}$) in mice receiving nano4-SRB. About half of AMs ingested nano4-SRB shown as $SRB^{+}DiD^{+}$, whereas DCs rarely captured the nanoparticles. The results were presented as means ± SEM. n=4 mice. The experiment was repeated twice with similar results.

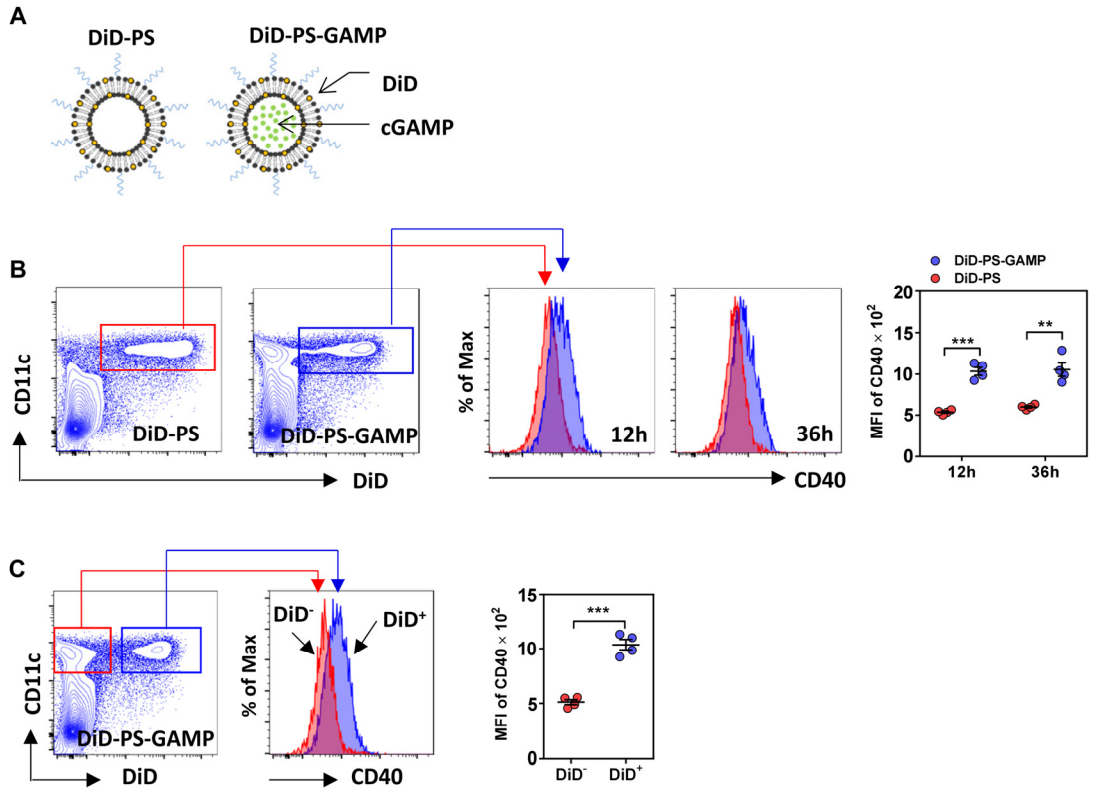

Fig. S5. Nano4 delivered cGAMP into AMs.

(**A**) Schematic diagrams of DiD-labeled empty PS-mimetic nanoparticles (DiD-PS) and cGAMP-encapsulated PS-mimetic nanoparticles (DiD-PS-GAMP). (**B**) DiD-PS or DiD-PS-GAMP (20 μg cGAMP) were i.n. inoculated. Pulmonary cells were analyzed for DiD^+ $CD11c^+$ cells by flow cytometry 12 or 36 h later in mice receiving DiD-PS (**Red**) or DiD-PS-GAMP (**Blue**). These cells were also assessed for CD40 expression to verify STING activation in the cells. Representative histogram of CD40 expression is given in the middle and Mean Fluorescence Intensity (MFI) is summarized in the right panel. n=4. (**C**) DiD^+ (**Blue**) or DiD^- AMs (**Red**) expressing CD40 were analyzed similarly as (**B**). n=4. The results were presented as means ± SEM. Each symbol represents individual mice in the right panels of **B** and **C**. Statistical analysis, *t*-test for (**B** and **C**). **p<0.01 and ***p<0.001 in the presence or absence of cGAMP. The experiment was repeated twice with similar results.

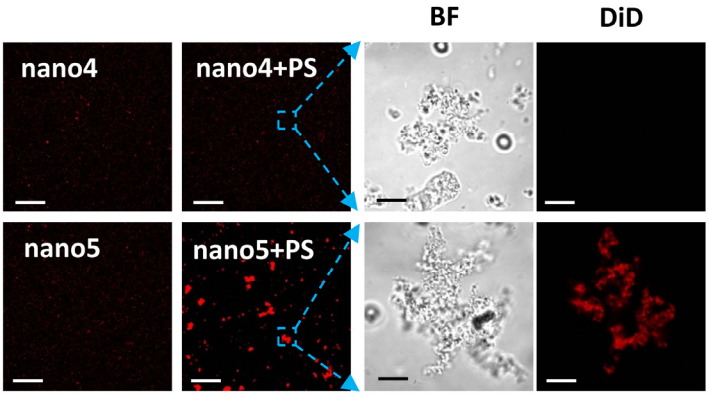

Fig. S6. Positively charged nano5 was entrapped by PS in ex vivo culture.
DiD-labeled Nano4 or nano5 was incubated with PS for 30 min. Nanoparticle aggregates on PS were visualized by confocal microscopy. The areas outlined in the 2nd panel were enlarged on the right. BF, Bright Field. Scale bar, 100 μm in panel 1 and 2 and 10 μm in panel 3 and 4. Data are representative of ten similar results in two separate experiments.

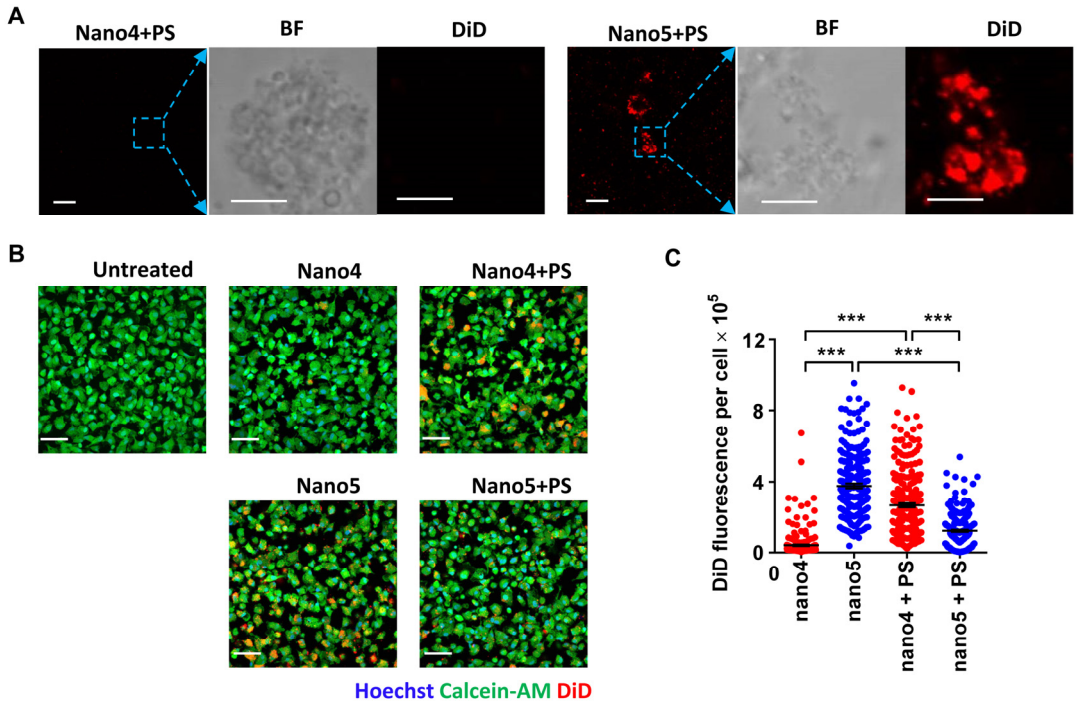

Fig. S7. Nano4 uptake by AMs isolated from non-human primates (NHP).

AMs and PS were isolated from rhesus macaques. (**A**) DiD-nano4 or DiD-nano5 was incubated for 30 min with rhesus macaque PS. Nano5, but not nano4, aggregated on PS and visualized by confocal microscopy. The areas outlined were enlarged in the corresponding panels on the right. Scale bar, 10 μm. Data are representative of five similar results. (**B**) Monkey AMs were isolated and cultured with DiD-nano4 (upper) or DiD-nano5 (low) for 3 h with or without PS pre-treatment of the nanoparticles and imaged by fluorescent microscopy. Live cells were stained by Calcein-AM and nuclei were stained by Hoechst. Scale bar, 50 μm. DiD fluorescence intensity in cells was quantified by Image J (**C**). n=221-275. Each symbol represents individual cells. The results were presented as means ± SEM. Statistical analysis, one-way ANOVA for (**C**). ***p<0.001 between indicated groups. We thank Prof. Wanli Liu, Dr. Junyi Wang, and Ms. Shaoling Qi for their help in the NHP study.

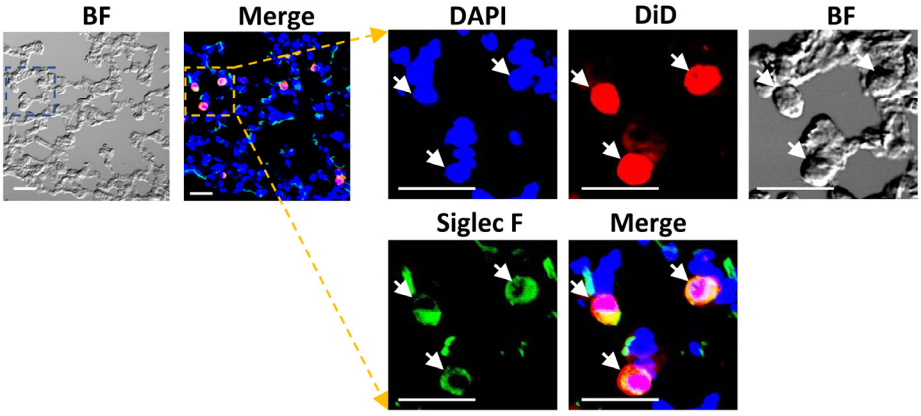

Fig. S8. AM capture nano4 in the lung.

Lungs were collected 12 h after mice received DiD-nano4 intranasally and frozen thin sections were stained for an AM-specific marker Siglec F and visualized by fluorescent microscopy. Scale bar, 30 μm. The square in the 2nd panel is enlarged on the right panels. Data are representative of six similar results in two separate experiments.

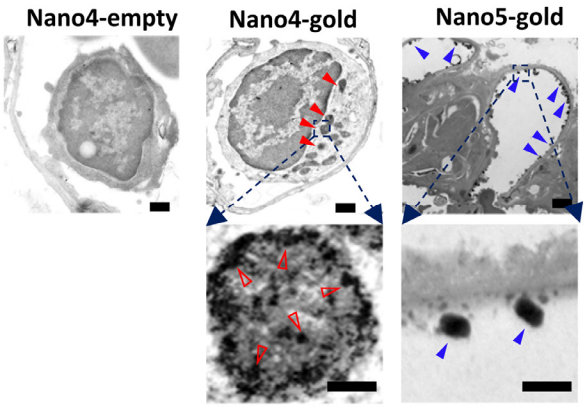

Fig. S9. TEM of nanoparticle distribution in the lung.

Nanogold was encapsulated within nano4 (nano4-gold) and nano5 (nano5-gold) as **Fig. S1A**. Mice were i.n. administered with the nanoparticles. Lungs were collected 6 h later and prepared for TEM. Note: nano4-gold was entrapped within cellular vesicles inside AM (**red** arrows) and some nanogolds were observed within a cellular vesicle (open red arrows, lower panel). In contrast, nano5-gold was mostly presented on the surface of alveoli (**blue** arrows). The areas outlined in upper panels are enlarged in the corresponding lower panels. Scale bar, 2 μm for the upper panel and 500 nm for the lower panel.

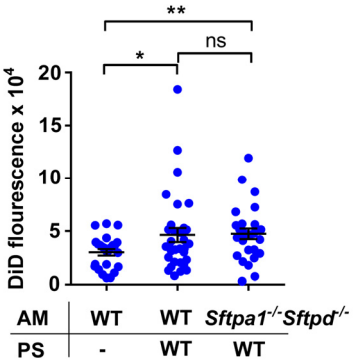

Fig. S10. AMs from *Sftpa1*$^{-/-}$*Sftpd*$^{-/-}$ mice had a similar capability as WT AMs in nano4 uptake.

SP-A/D are hydrophilic large proteins and well established as a first line of the innate defense. These two collectins are capable of integrating into PS-wrapped bacteria, viruses, cellular debris, apoptotic cells, and various nanoparticles, to facilitate their endocytosis or phagocytosis by AMs (*20*). To test whether this might be the mechanism for nano4 uptake by AMs, AMs were isolated from WT or *Sftpa1*$^{-/-}$*Sftpd*$^{-/-}$ mice and incubated with DiD-nano4 that was pre-treated with WT PS for 30 min. DiD fluorescence in cells was captured by confocal microscopy and quantified by Image J software. AMs from *Sftpa1*$^{-/-}$*Sftpd*$^{-/-}$ mice were found to ingest nano4 as efficiently as WT AMs in the presence of WT PS, but not in the presence of SP-A/D-deficient PS (**Fig. 1I**). n=25-32. Each symbol represents individual cells. Statistical analysis, one-way ANOVA. *p<0.05 and **p<0.01 between indicated groups and ns, not significant. The experiment was repeated twice with similar results.

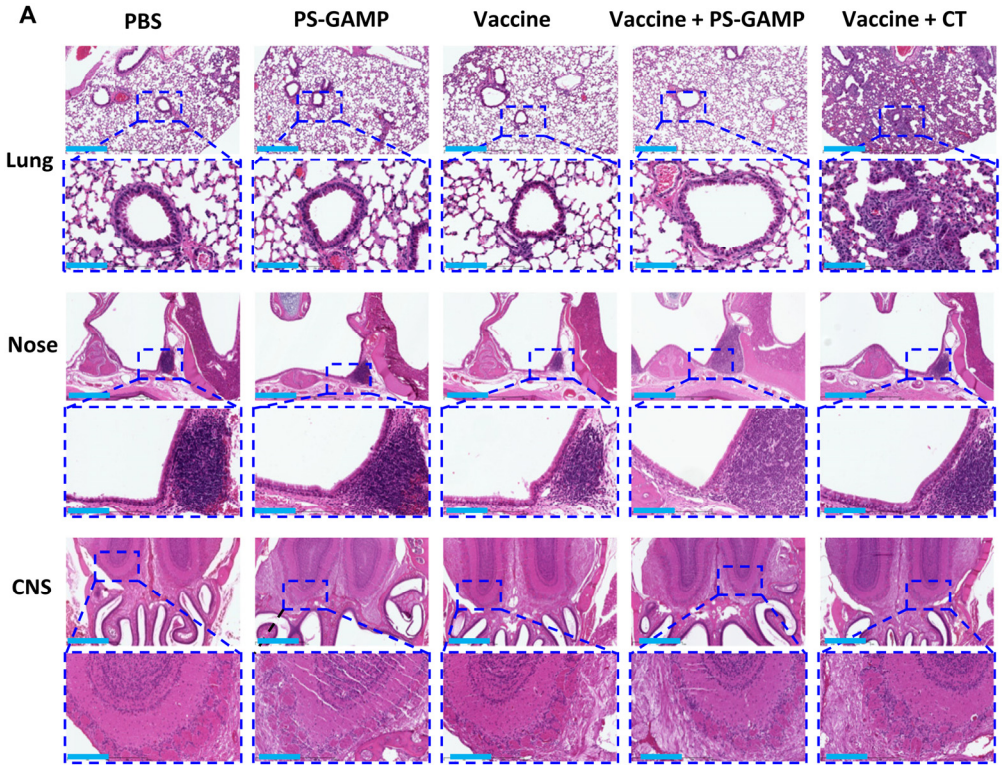

B

Summary of histopathological analysis

	Lung						Nose						CNS			
	Eosinophil infiltrates		Alveolar damage		Necrosis		Eosinophil infiltrates		Epithelium damage		Necrosis		Eosinophil infiltrates		Necrosis	
Treatment	+	–	+	–	+	–	+	–	+	–	+	–	+	–	+	–
PBS	0	6	0	6	0	6	0	6	0	6	0	6	0	6	0	6
PS-GAMP	0	6	0	6	0	6	0	6	0	6	0	6	0	6	0	6
Vaccine	0	6	0	6	0	6	0	6	0	6	0	6	0	6	0	6
Vaccine+PS-GAMP	0	6	0	6	0	6	0	6	0	6	0	6	0	6	0	6
Vaccine+CT	6	0	6	0	6	0	1	5	1	5	2	4	0	6	0	6

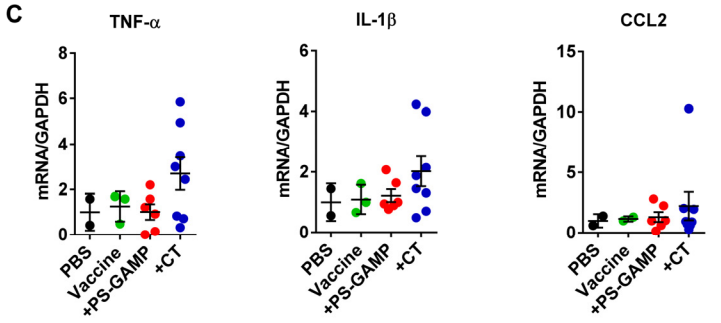

Fig. S11. PS-GAMP did not induce overt inflammation in the lung, nose, and central nervous system (CNS).

Swiss Webster mice were i.n. administered with PBS, PS-GAMP, VN04 H5N1 vaccine, or the vaccine plus PS-GAMP or CT. (**A**) Histological examination of the lung (1st and

2nd panel), nose (3rd and 4th panel), and CNS (5th and 6th panel) in 2 d post-immunization. Alveolar and bronchus of lungs, the nasal associated lymphoid tissue of noses, and the olfactory bulb region of the brain tissue are outlined by a dashed rectangle and enlarged in the corresponding bottom panels. The olfactory bulb region of the brain tissue connects directly with olfactory nerves in the nasal cavity. Data are representative of two separate experiments each assayed in triplicate. Scale bars for the lung and nose, the upper panel 400 μm and the lower panel 100 μm. Scale bars for CNS, the upper panel 800 μm and the lower panel 200 μm. (**B**) Eosinophil infiltrates, epithelium damage, and necrosis of each mouse were analyzed as previously reported (*48*). The number indicates the number of mice with (+) or without (−) eosinophil infiltrates, epithelium damage or necrosis. n=6 mice. (**C**) Expression of indicated cytokines and chemokine in the CNS of mice receiving VN04 H5N1 vaccine in the presence or absence of PS-GAMP or CT was determined by real-time RT-PCR 2 d post-immunization. n=2-8. Each symbol represents individual mice. The results were presented as means ± SEM.

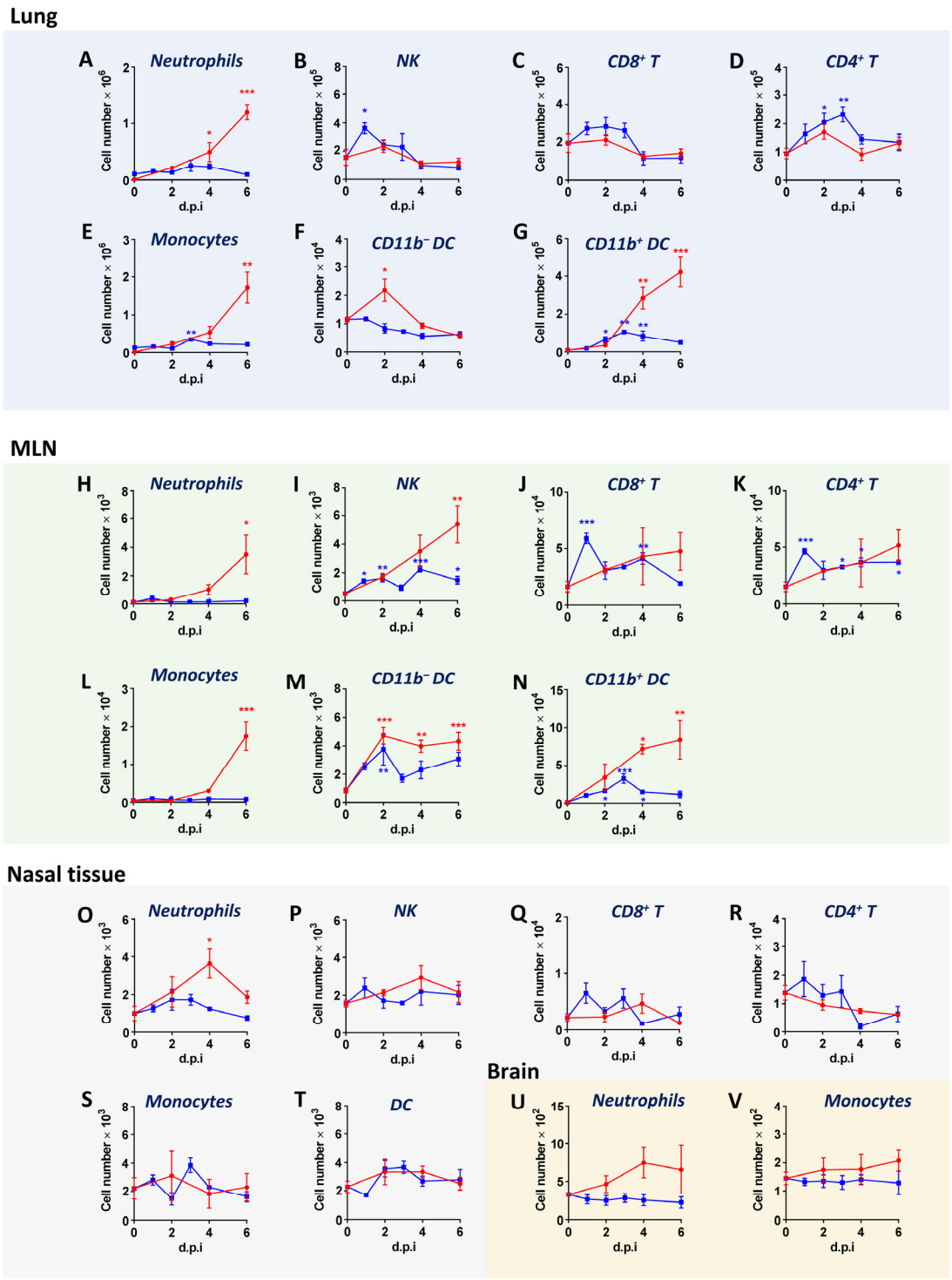

Fig. S12. Alterations of inflammatory and immune cells after PS-GAMP administration or viral infection.

C57BL6 mice were i.n. administered with CA09 H1N1 vaccine plus 20 μg of PS-GAMP (**Blue**) or infected with 1×LD_{50} CA09 H1N1 influenza virus (**Red**). Neutrophils, NK,

$CD4^+$, and $CD8^+$ T cells, monocytes, and $CD11b^+$ and $CD11b^-$ DCs in the lung (**A** to **G**) or MLN (**H** to **N**) were analyzed by flow cytometry on indicated d post-infection or post-immunization (d.p.i). Neutrophils, NK, $CD4^+$, and $CD8^+$ T cells, monocytes and DCs in nasal tissue (**O** to **T**) or neutrophils and monocytes in brain (**U** and **V**) were similarly analyzed. n=4. The results were presented as means ± SEM. Statistical analysis, one-way ANOVA. *p<0.05, **p<0.01, and ***p<0.001 compared to d 0. The experiment was repeated twice with similar results.

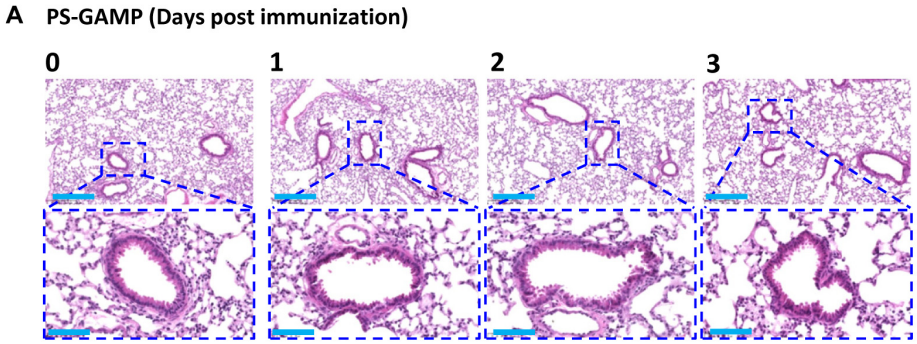

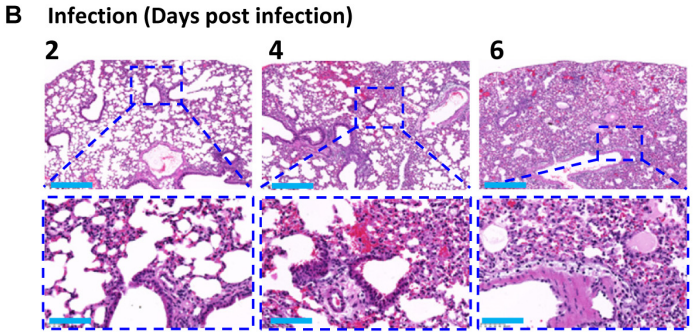

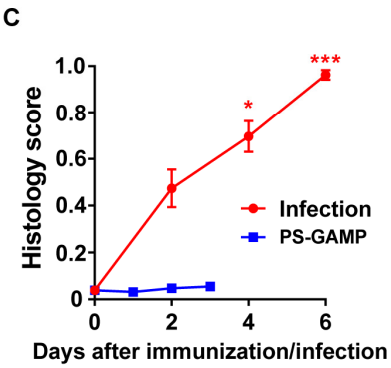

Lung Injury Soring System

Parameter	Score per field 0	1	2
A. Neutrophils in the alveolar space	None	1-5	>5
B. Neutrophils in the interstitial space	None	1-5	>5
C. Hyaline membranes	None	1	>1
D. Proteinaceous debris filling the airspaces	None	1	>1
E. Alveolar septal thickening	<2x	2x-4x	>4x

Score = [(20 × A) + (14 × B) + (7 × C) + (7 × D) + (2 × E)]/(number of fields × 100)

Fig. S13. PS-GAMP did not induce overt inflammation in the lung in contrast to viral infection.

Mice were i.n. immunized with CA09 H1N1 vaccine plus 20 μg of PS-GAMP (**A**) or infected with 1×LD_{50} CA09 H1N1 influenza virus (**B**). Lungs were analyzed by H&E staining on indicated d after immunization or infection. Data are representative of two separate experiments each assayed in triplicate. Scale bar, 400 μm for upper panel and 100 μm for lower panel. (**C**) The lung inflammation was quantified according to a standard scoring system shown on the right (*49*). n=6. Data were presented as means ± SEM. *p<0.05 and ***p<0.001 compared to d 0 by Kruskal-Wallis test.

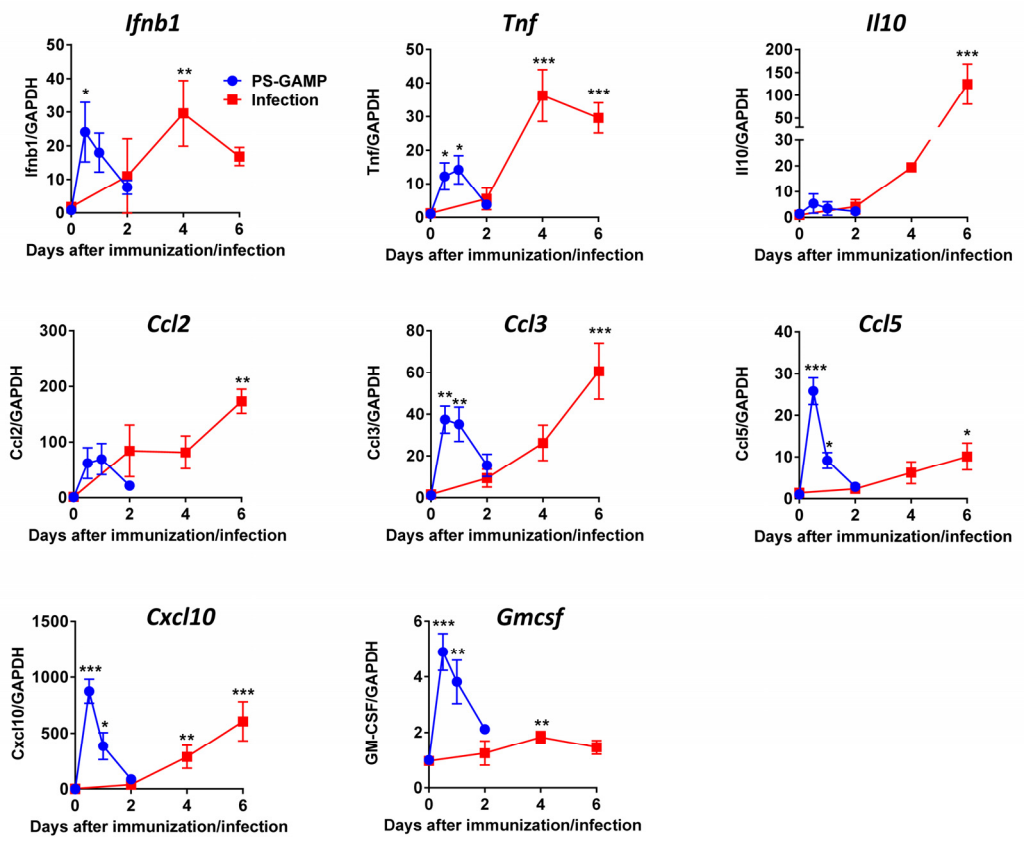

Fig. S14. PS-GAMP induces transient production of immune mediators in the lung. Mice were i.n. given 20 μg of PS-GAMP (**Blue**) or infected with 1×LD_{50} CA09 H1N1 influenza virus (**Red**). mRNA levels of indicated mediators were measured by real-time RT-PCR at various time points and normalized against untreated mice. n=4. The results were presented as means ± SEM. Statistical analysis, one-way ANOVA. *p<0.05, ** p<0.01, and ***p<0.001 compared to d 0. The experiment was repeated twice with similar results.

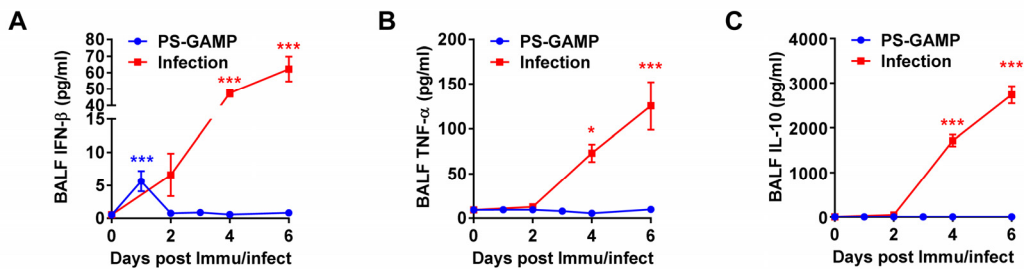

Fig. S15. PS-GAMP briefly elevates IFN-β protein in BALF.

Mice were i. n. administered 20 μg of PS-GAMP (**Blue**) or infected with 1×LD_{50} CA09 H1N1 influenza virus (**Red**). Protein levels of IFN-β (**A**), TNF-α (**B**), and IL-10 (**C**) in BALF were measured by ELISA at various time points. n=4. The results were presented as means ± SEM. Statistical analysis, one-way ANOVA. *p<0.05 and ***p<0.001 compared to d 0 (before treatments). The experiment was repeated twice with similar results.

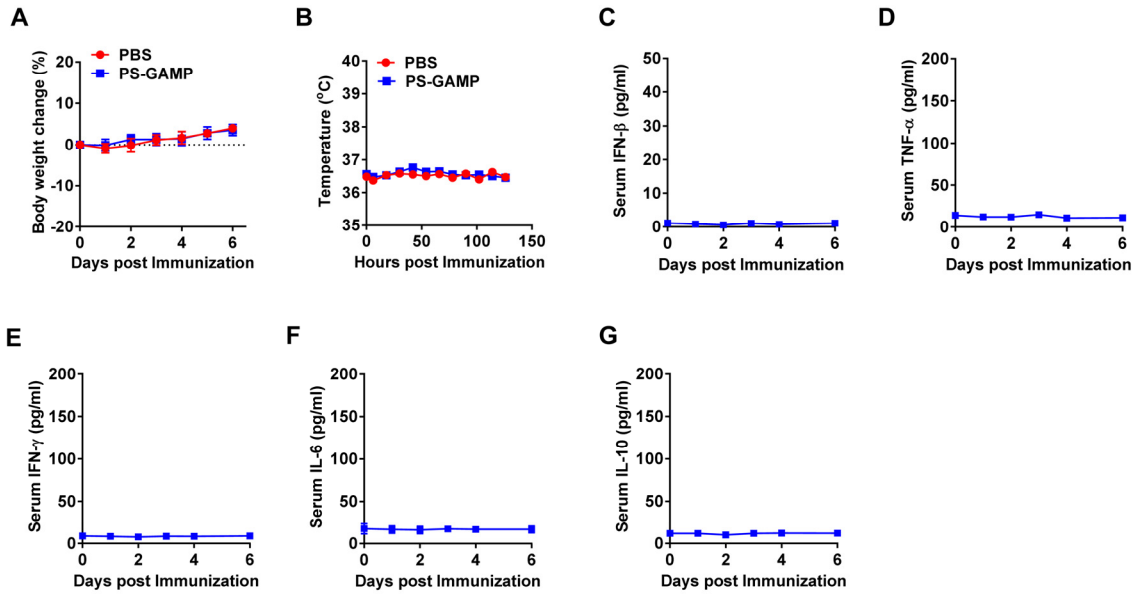

Fig. S16. PS-GAMP did not induce any inflammation systemically.

Mice were i.n. immunized with CA09 H1N1 vaccine plus 20 μg of PS-GAMP. Body weight (**A**) and temperature (**B**) were monitored for 6 d. Mice receiving PBS served as control. n=5. Serum IFN-β (**C**), TNF-α (**D**), IFN-γ (**E**), IL-6 (**F**), and IL-10 (**G**) were also monitored for 6 d by ELISA. n=4. The results were presented as means ± SEM. The experiment was repeated twice with similar results.

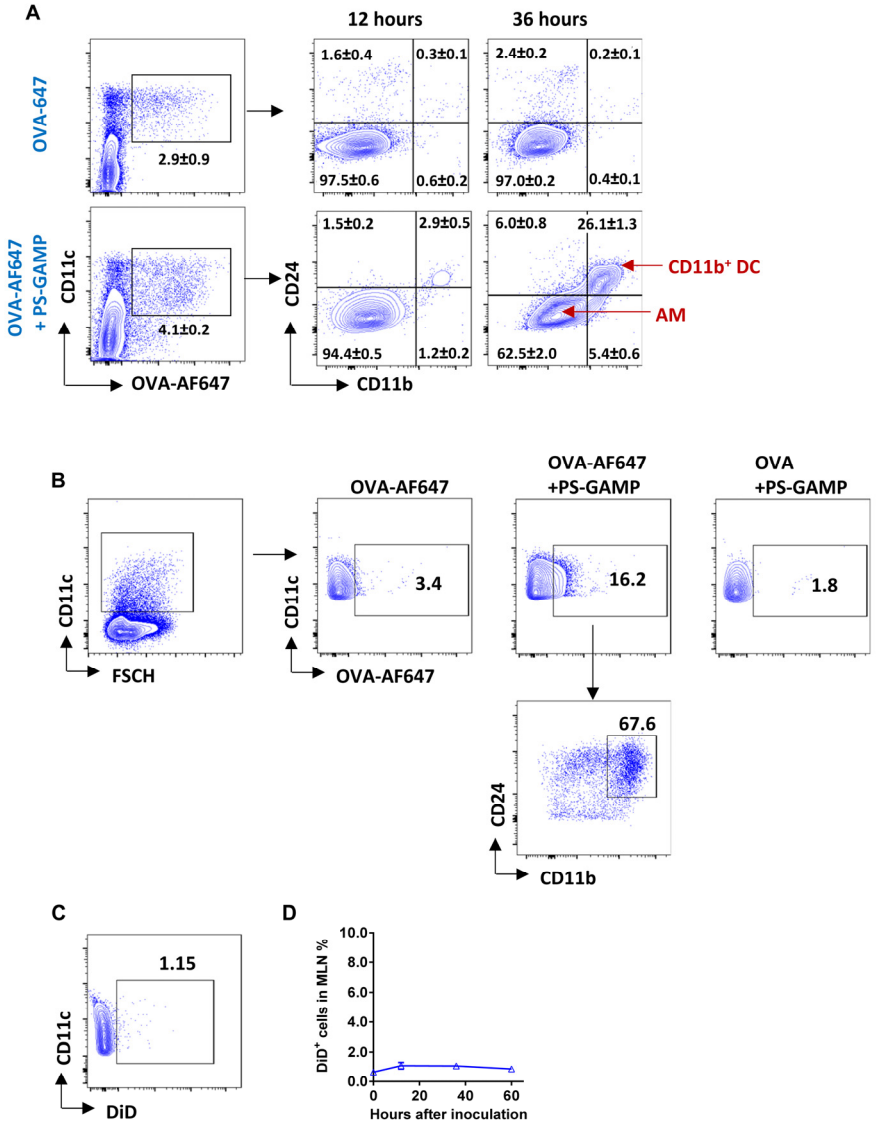

Fig. S17. PS-GAMP increases the number of CD11b$^+$ DCs ingesting extracellular Ag in the lung and MLN.

(**A**) Mice were i.n. vaccinated with OVA-AF647 with or without 20 μg of PS-GAMP. Pulmonary CD11c$^+$ cells capturing OVA were analyzed for CD11b and CD24 expression. The numbers in the plots are mean percentages ± SEM of individual cell subsets. (**B**) Mice receiving OVA (non-fluorescence) + PS-GAMP served as controls to gate out cell activation-related autofluorescence. OVA uptake was analyzed 36 h later on the gate of DCs prepared from MLNs revealing OVA$^+$ DCs to be mostly CD11b$^+$ DCs. (**C**) DCs did not directly ingest PS-GAMP in the MLN as shown by few CD11c$^+$DiD$^+$ cells when mice were i.n. administered with 20 μg of DiD-PS-GAMP and analyzed similarly. (**D**) DiD$^+$ cells were also tracked in MLNs from 0 to 60 h after PS-GAMP administration. n=4. The results were presented as means ± SEM. The experiment was repeated twice with similar results.

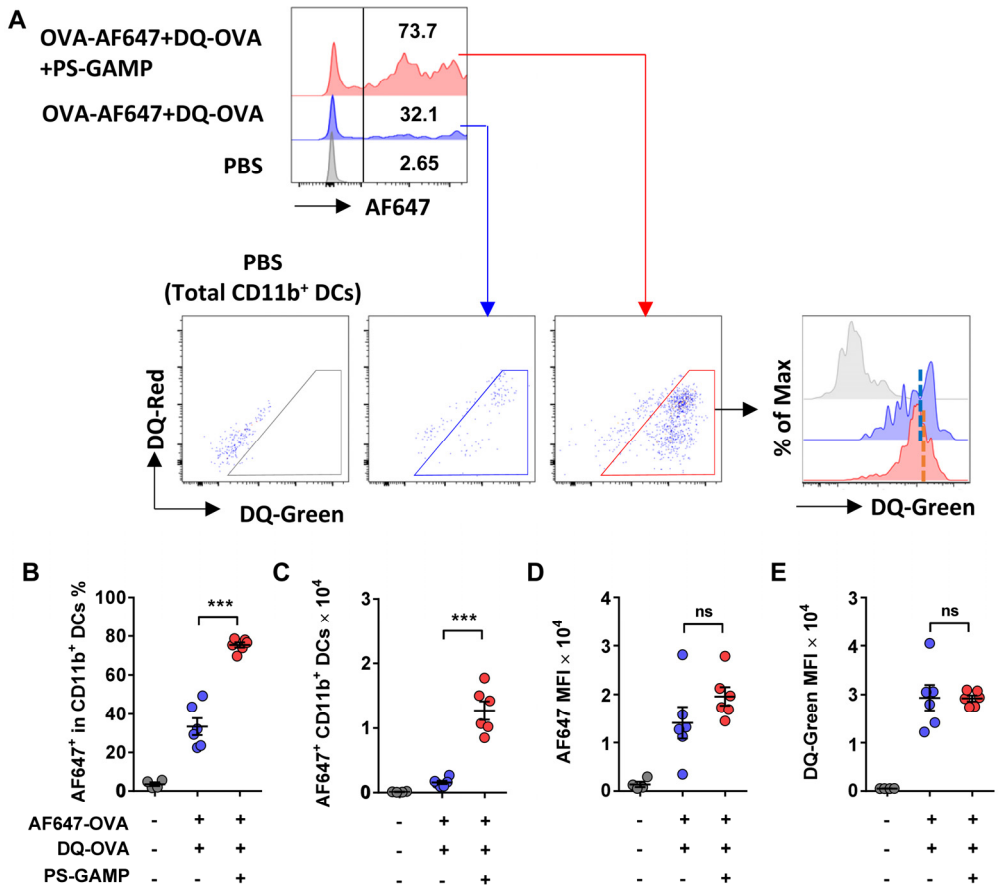

Fig. S18. PS-GAMP did not augment Ag-uptake or processing in vivo.

Whether PS-GAMP influenced Ag-uptake or Ag-processing was evaluated using AF647-labeled OVA and DQ-OVA. DQ-OVA is OVA conjugation with a BODIPY fluorescent dye (DQ) and remains self-quenched until OVA is proteolytically processed to generate DQ-green fluorescence, which is commonly used to assess Ag-processing. To this end, mice were i.n. administered with PBS (**Gray**) or AF647-OVA together with DQ-OVA in the presence (**Red**) or absence (**Blue**) of PS-GAMP and euthanized 24 h later for flow cytometric analysis (**A**). AF647-OVA was analyzed on the gate of DC11b$^+$ DCs, which were further quantified for OVA cleavage based on DQ-green fluorescence. Percentages and cell numbers of AF647$^+$ CD11b$^+$ DCs were summarized in (**B**) and (**C**). AF647 and DQ-Green MFIs in these cells were given in (**D**) or (**E**), respectively. Each symbol represents individual mice in **B** to **E**. The results were presented as means ± SEM. Statistical analysis, one-way ANOVA for (**B-E**). *p<0.05, **p<0.01, and ***p<0.001 in the presence or absence of PS-GAMP. ns, no significance. The experiment was repeated twice with similar results. **Note:** there was no difference in MFI of DQ-green fluorescence or OVA in AF647$^+$CD11b$^+$ DCs irrespective of whether or not PS-GAMP was presented (**D** and **E**). However, percentages and numbers of CD11b$^+$ DCs positive to OVA were robustly increased in the presence of PS-GAMP (**B** and **C**), which was attributed primarily from an increased number of CD11b$^+$ DCs secondarily to immune mediators induced by PS-GAMP.

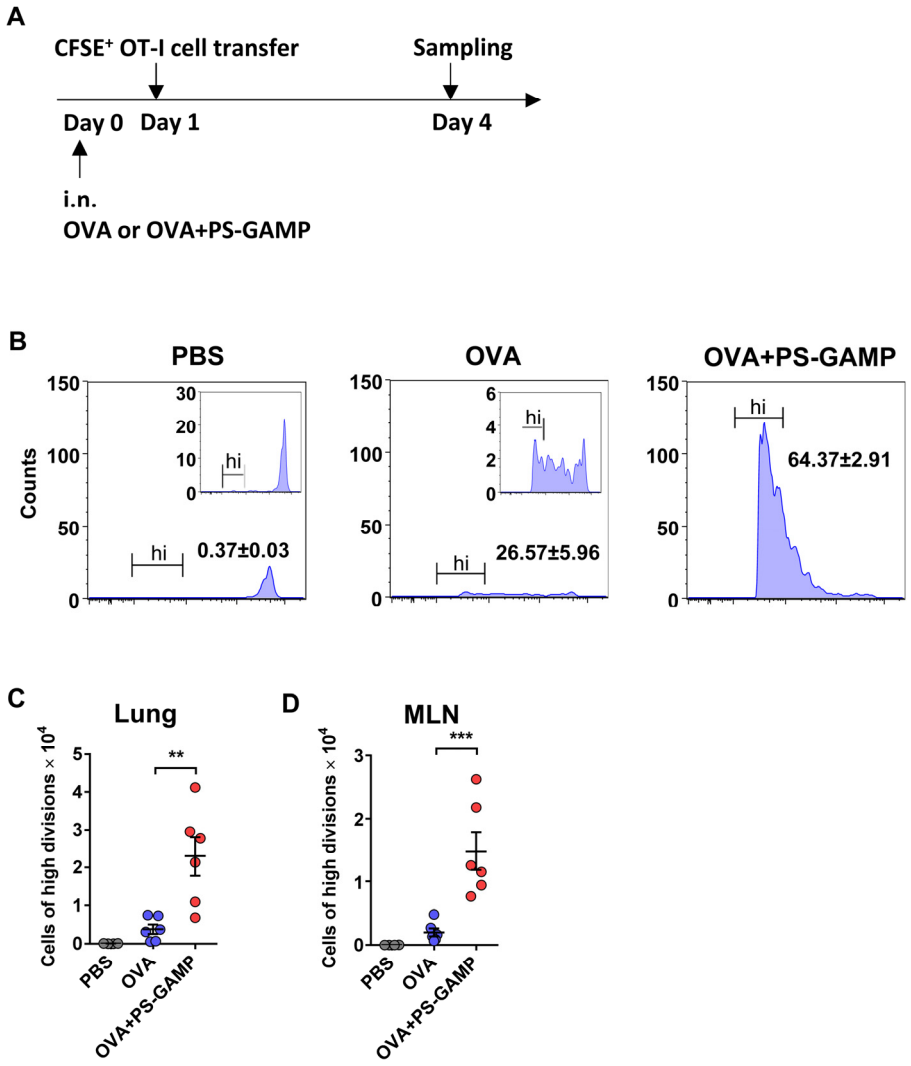

Fig. S19. PS-GAMP enhances Ag cross-presentation.

(**A**) Mice were i.n. vaccinated with 60 μg of OVA with or without 20 μg of PS-GAMP. Carboxyfluorescein succinimidyl ester (CFSE)-labeled OT-I cells were transferred into vaccinated mice 1 d later. Lungs and MLN were collected 3 d post-cell transfer. (**B**) OT-I cells were analyzed for Ag-specific proliferation by step-wise decreases of CFSE fluorescence. Inset in the first two panels (PBS and OVA): a reduced scale of the y-axis to show CFSE decreases. Cells of high divisions (≥6, hi) were gated. Numbers of highly divided cells in lungs (**C**) and MLNs (**D**) were summarized. n=4-6. Each symbol represents individual mice in **C** and **D**. Statistical analysis, one-way ANOVA for (**C** and **D**). The results were presented as means ± SEM. **p<0.01 and ***p<0.001 in the presence or absence of PS-GAMP. The experiment was repeated twice with similar results.

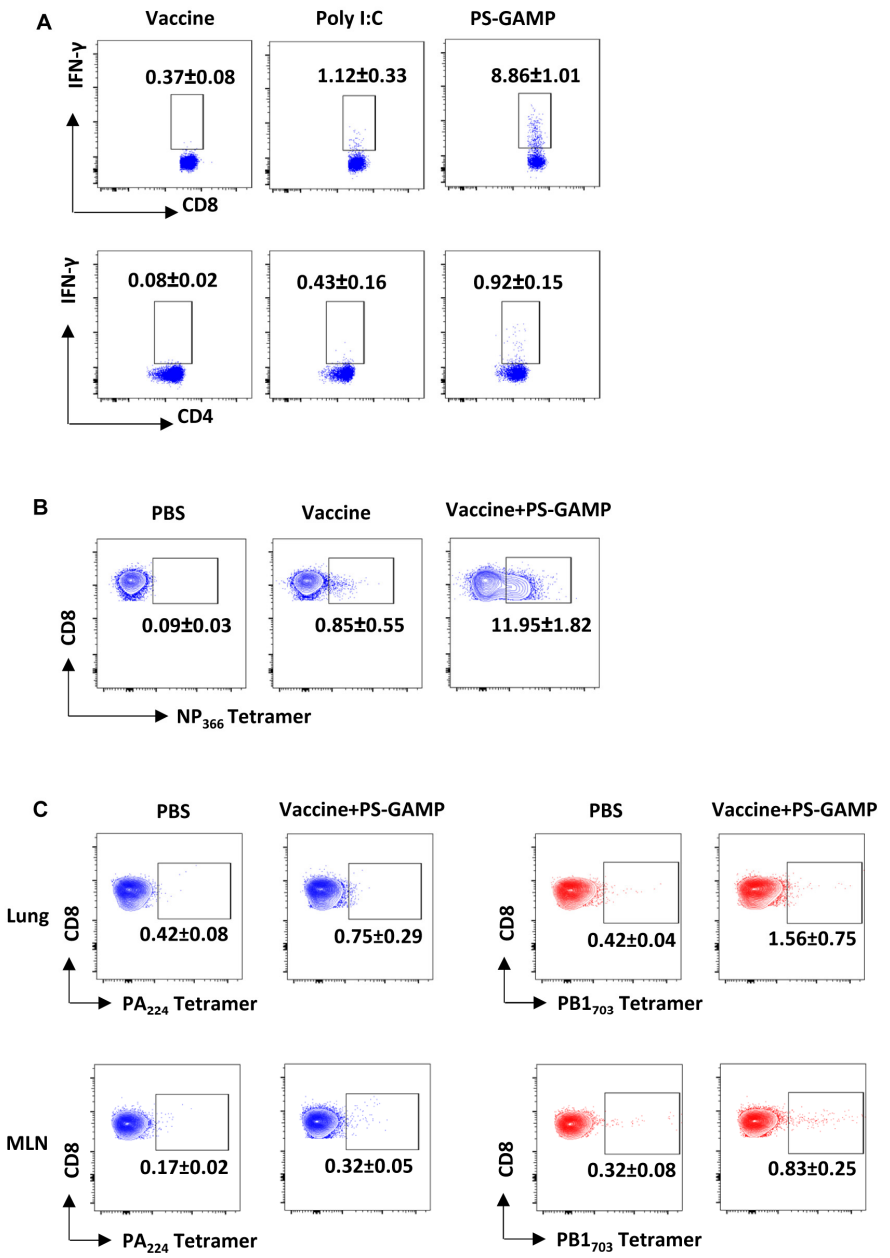

Fig. S20. CD8$^+$ T cell responses in the spleen, lung and MLN.

C57BL/6 mice were i.n. immunized with CA09 H1N1 vaccine plus 20 μg of PS-GAMP. Mice received PBS as a control. (**A**) Splenocytes were isolated 7 d post-immunization and stimulated with the CA09 H1N1 vaccine. Representative cytometric profiles of CD4$^+$ and CD8$^+$ T cells producing IFN-γ are shown. (**B**) Representative cytometric profiles of NP$_{366\text{-}374}^+$ CD8$^+$ T cells in the lung 4 d after immunization. (**C**) Percentages of PA$_{224\text{-}233}$ (**Blue**) or PB1$_{703\text{-}711}$ (**Red**) positive cells were determined on gate of CD3$^+$CD8$^+$ T cells. Each plot is representative of four similar results in the same group. n=4. Data are presented as means ± SEM. The experiment was repeated twice with similar results.

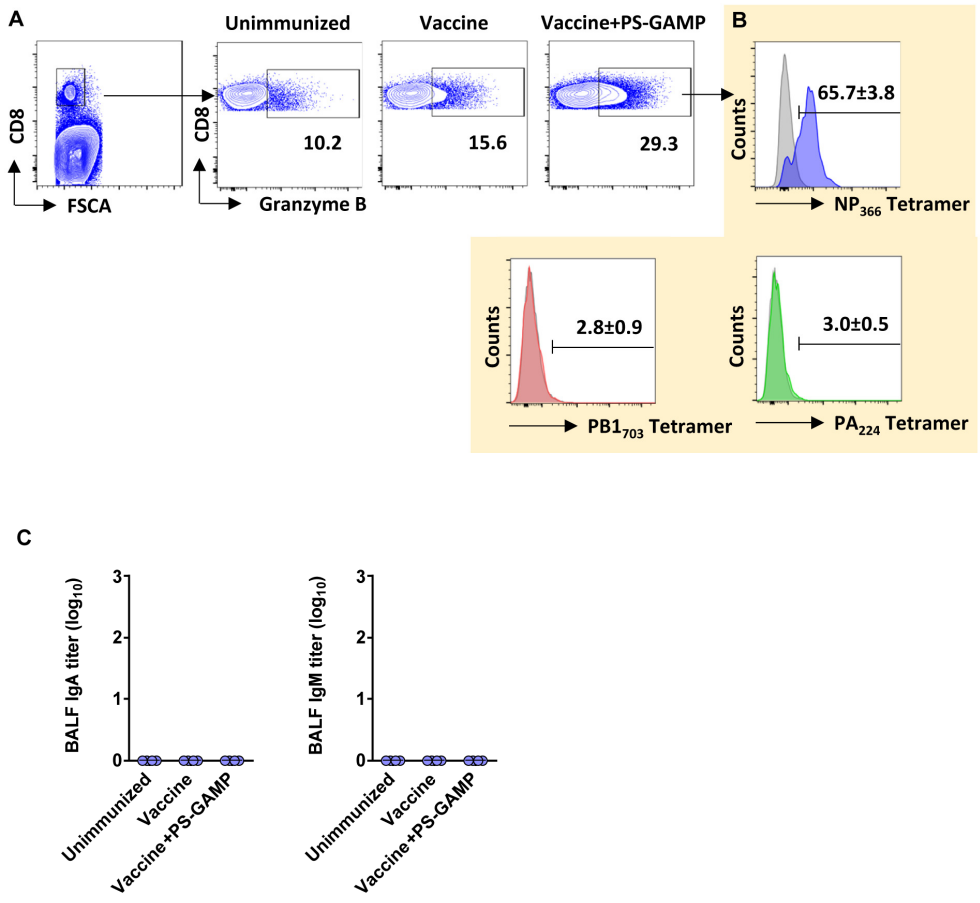

Fig. S21. Early viral specific GZMB$^+$CD8$^+$ T cells and BALF antibodies.

(**A**) C57BL/6 mice were either left unimmunized or immunized with CA09 H1N1 vaccine alone or the vaccine plus 20 μg of PS-GAMP, followed 2 d later by challenging with 10×LD_{50} CA09 H1N1 virus. Lungs were collected 4 d post-infection. (**B**) The percentages of $NP_{366\text{-}374}$ tetramer (**Blue**), $PB1_{703\text{-}711}$ (**Red**), or $PA_{224\text{-}233}$ (**Green**) positive cells were obtained on the gate of GZMB$^+$CD8$^+$ T cells. CD8$^+$ T cells from un-immunized/un-challenged mice were analyzed in parallel as negative controls (**Gray**). n=3. (**C**) BALF were analyzed for Ag-specific IgA and IgM titers 6 d post-immunization. n=4. Data are presented as means ± SEM. The experiment was repeated twice with similar results.

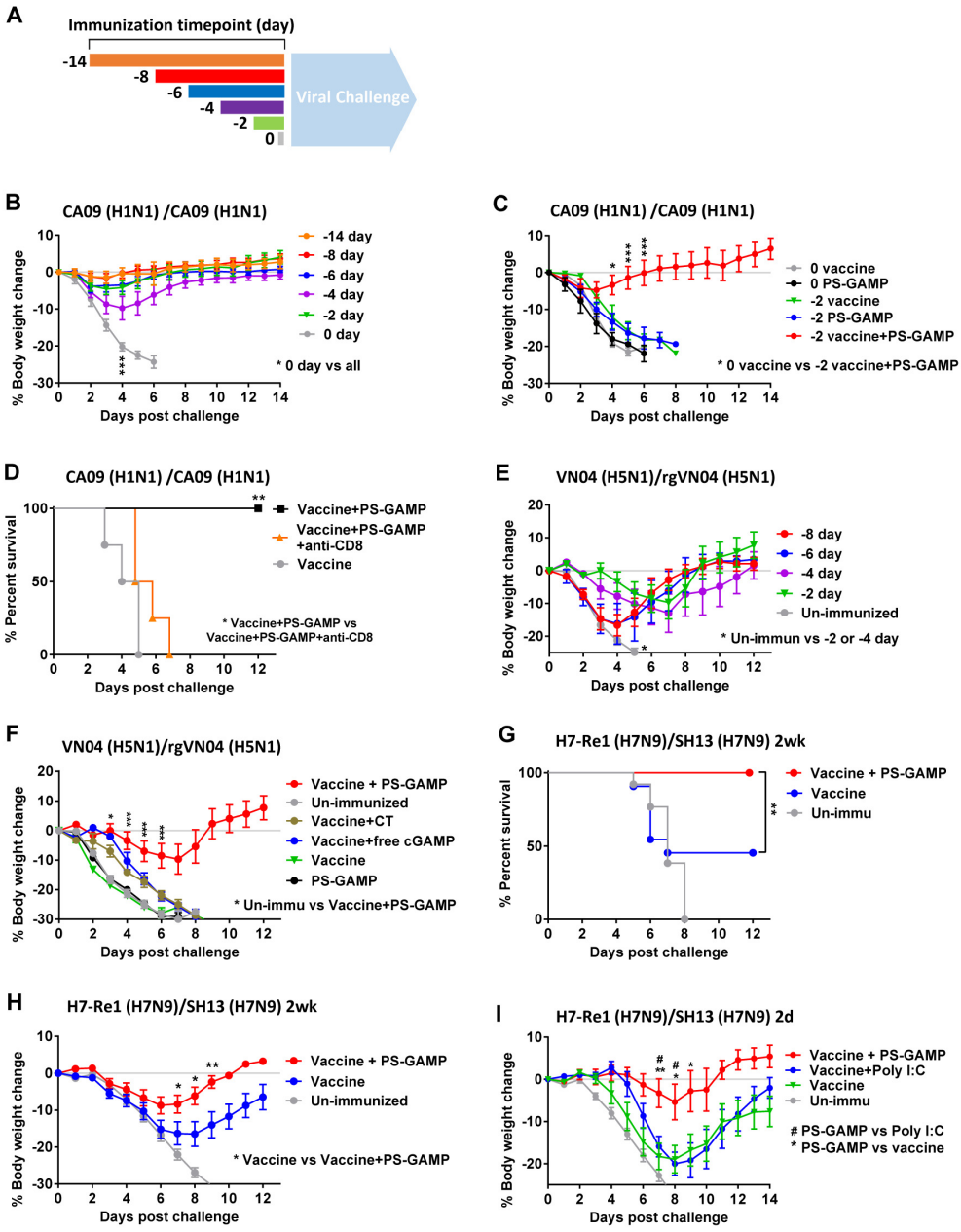

Fig. S22. Supplementary data for Fig. 4.

(**A**) A schematic diagram of vaccination and viral challenge schedule. (**B** to **F**) The body weight changes (**B**, **C**, **E**, and **F**) or survival (**D**) of mice corresponding to those described in **Fig. 4**, **A** to **E**, respectively. (**G** and **H**) Mice were i.n. immunized with H7-Re1 H7N9 vaccine alone or alongside 20 μg of PS-GAMP or poly I:C and challenged 14 d later by a clinically isolated SH13 H7N9 virus. n=10-13. (**I**) Body weight change of mice described in **Fig. 4F**. Statistical analysis, two-way ANOVA for (**B, C, E, F, H, I**), Log-rank test for (**D** and **G**). *p< 0.05, **p<0.01, ***p<0.001, and #p<0.05. All experiments were repeated at least twice with similar results.

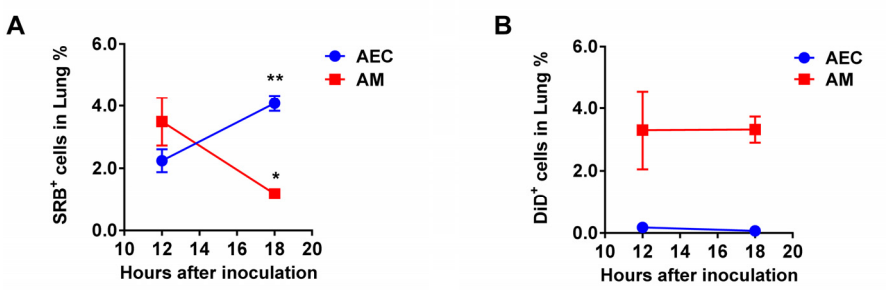

Fig. S23. An inverse correlation of SRB$^+$AMs vs. SRB$^+$AECs over time in vivo while DiD$^+$AMs remained unaltered in percentages.

SRB-DiD-nano4 was i.n. inoculated into mice. (**A**) Percentage changes of SRB$^+$AMs and SRB$^+$AECs relative to a total number of lung cells were tracked over time after the inoculation. n=4. (**B**) DiD$^+$ AMs were analyzed by flow cytometry 12 and 18 h later following nanoparticle administration. n=4. The results were presented as means ± SEM. Statistical analysis, *t*-test. *p<0.05 and **p<0.01 compared between 18 and 12 h. All experiments were repeated twice with similar results.

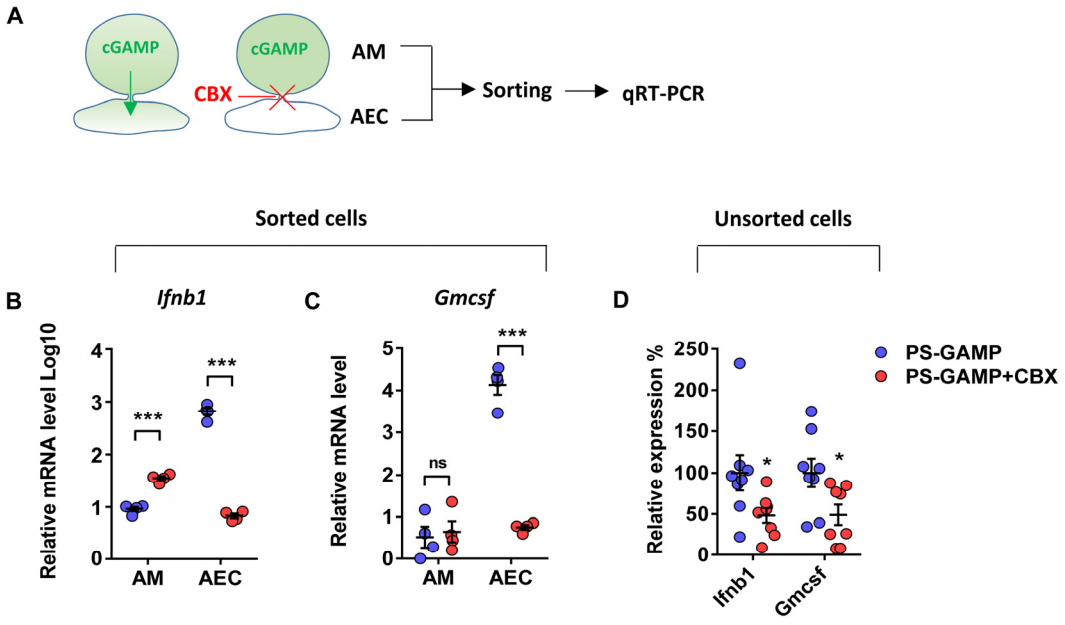

Fig. S24. Entry of cGAMP from AMs into AECs.

(**A**) Mice were i.p. injected with a gap junction inhibitor CBX or PBS for 3 consecutive d, after which 20 μg of PS-GAMP was i.n. administrated. AMs and AECs were sorted 12 h later and analyzed for *Ifnb1* (**B**) and *Gmcsf* (**C**) expression by real-time RT-PCR. mRNA levels were first normalized to *Gapdh* and then to corresponding cells isolated from naïve mice. n=4. (**D**) Unsorted lung cells were also analyzed similarly for comparisons. n=8. The results were presented as means ± SEM. Each symbol represents individual mice in **B** to **D**. Statistical analysis, *t*-test. *p<0.05 and ***p<0.001 in the presence or absence of CBX. ns, no significance. All experiments were repeated twice with similar results.

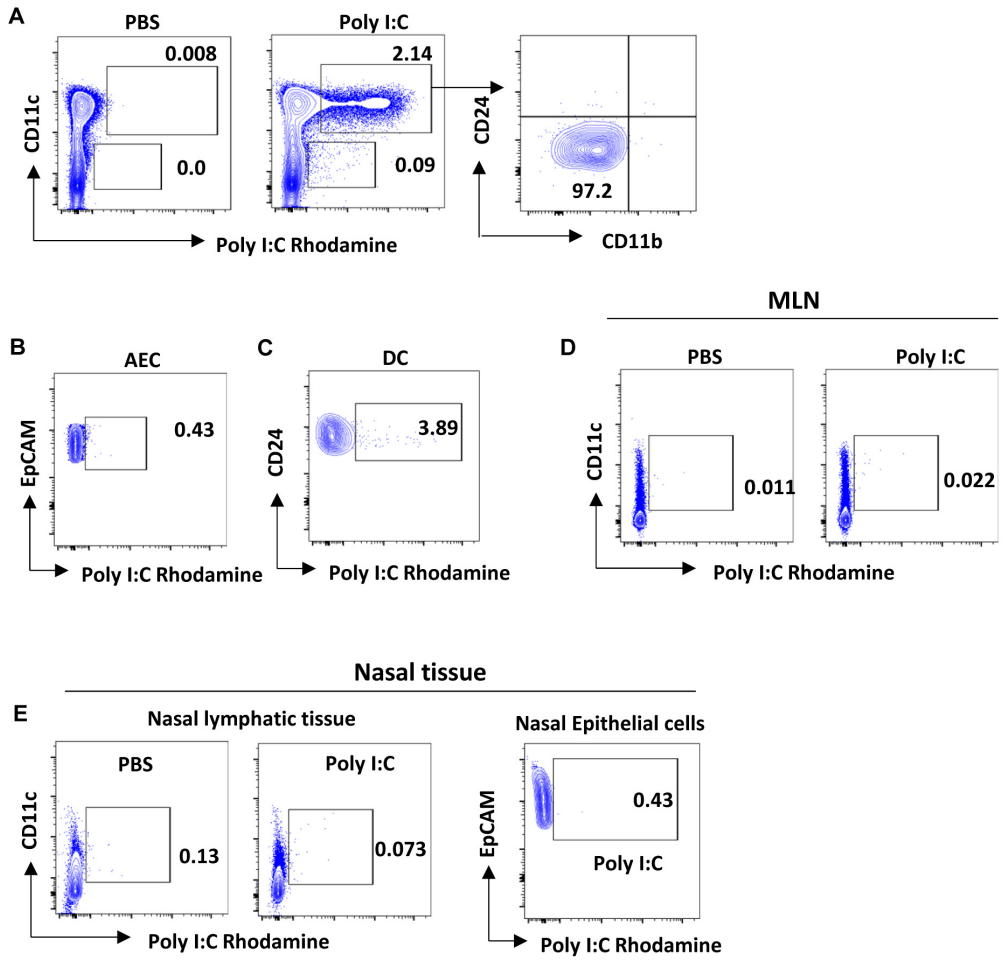

Fig. S25. Tissue and cell distribution of poly I:C.

Mice received 20 µg of rhodamine-labeled poly I:C intranasally. (**A**) Lungs were dissected and digested 12 h later for flow cytometric analysis of poly I:C uptake by $CD11c^+$ and $CD11c^-$ subsets. $CD11c^+$poly $I:C^+$ cells were further confirmed to be $CD24^-$ $CD11b^-$ AMs. Poly I:C uptake was next analyzed on the gate of $EpCAM^+$ AECs (**B**) or $CD11c^+CD24^+$ DCs (**C**). MLNs (**D**) and nasal epithelium and lymphatic tissue (**E**) were also prepared for single-cell suspensions to determine poly I:C uptake. Data are representative of two separate experiments each assayed in triplicate.

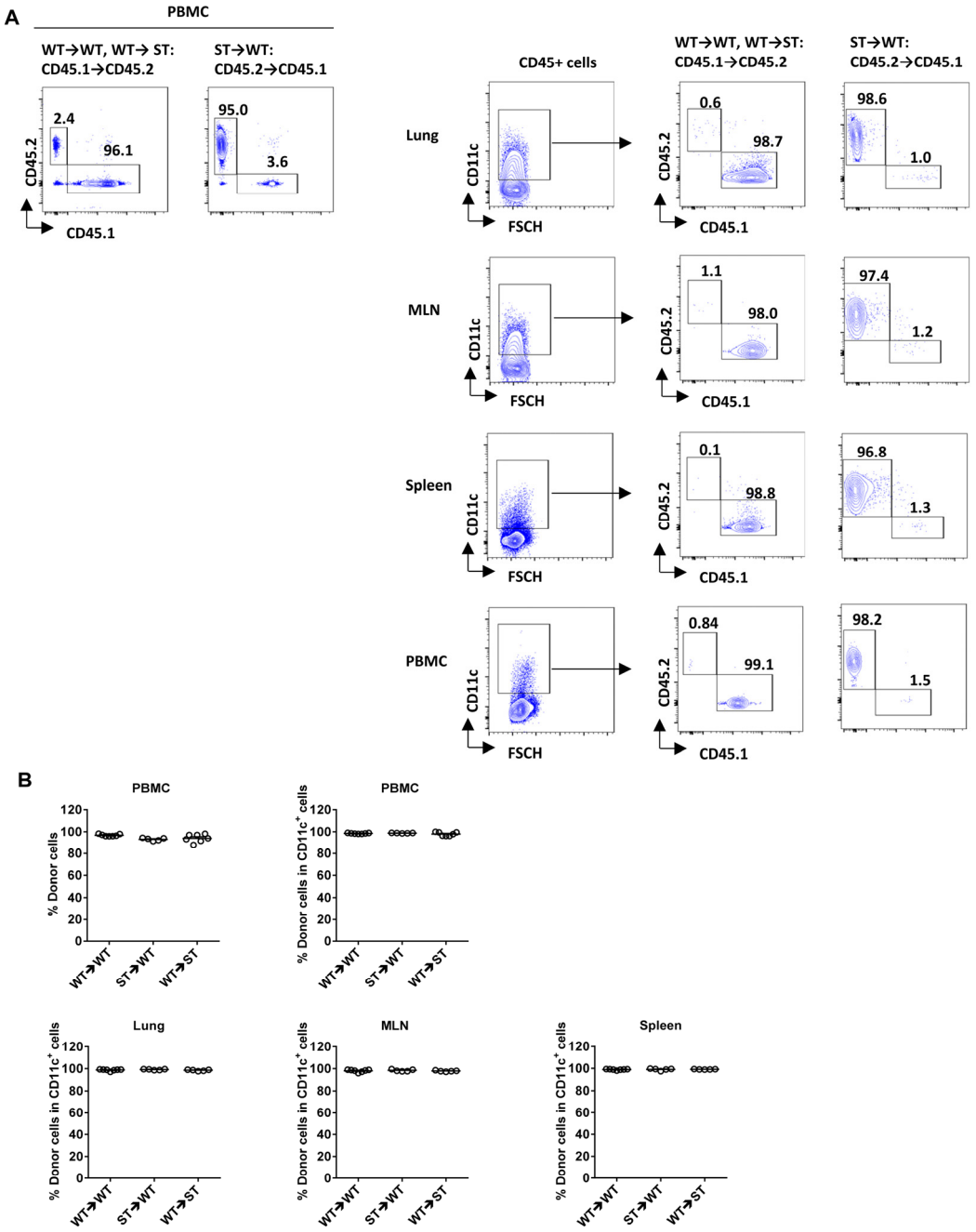

Fig. S26. Cell reconstitution efficacy after bone marrow (BM) cell transfer.

Mice were pre-conditioned with lethal irradiation prior to infusion with BM cells isolated from mice carrying reciprocal CD45 alleles, CD45.1 and CD45.2, a surface biomarker for all leukocytes. Donor cells were distinguished from recipients by a specific antibody for CD45.1 or CD45.2. The transfer efficacy was analyzed by quantifying CD45.1 or CD45.2 expression on leukocytes in various tissues in the recipients after three months of infusion (**A**) and summarized in (**B**). Each symbol represents individual mice in (**B**). n=5-7. The experiment was repeated twice with similar results.

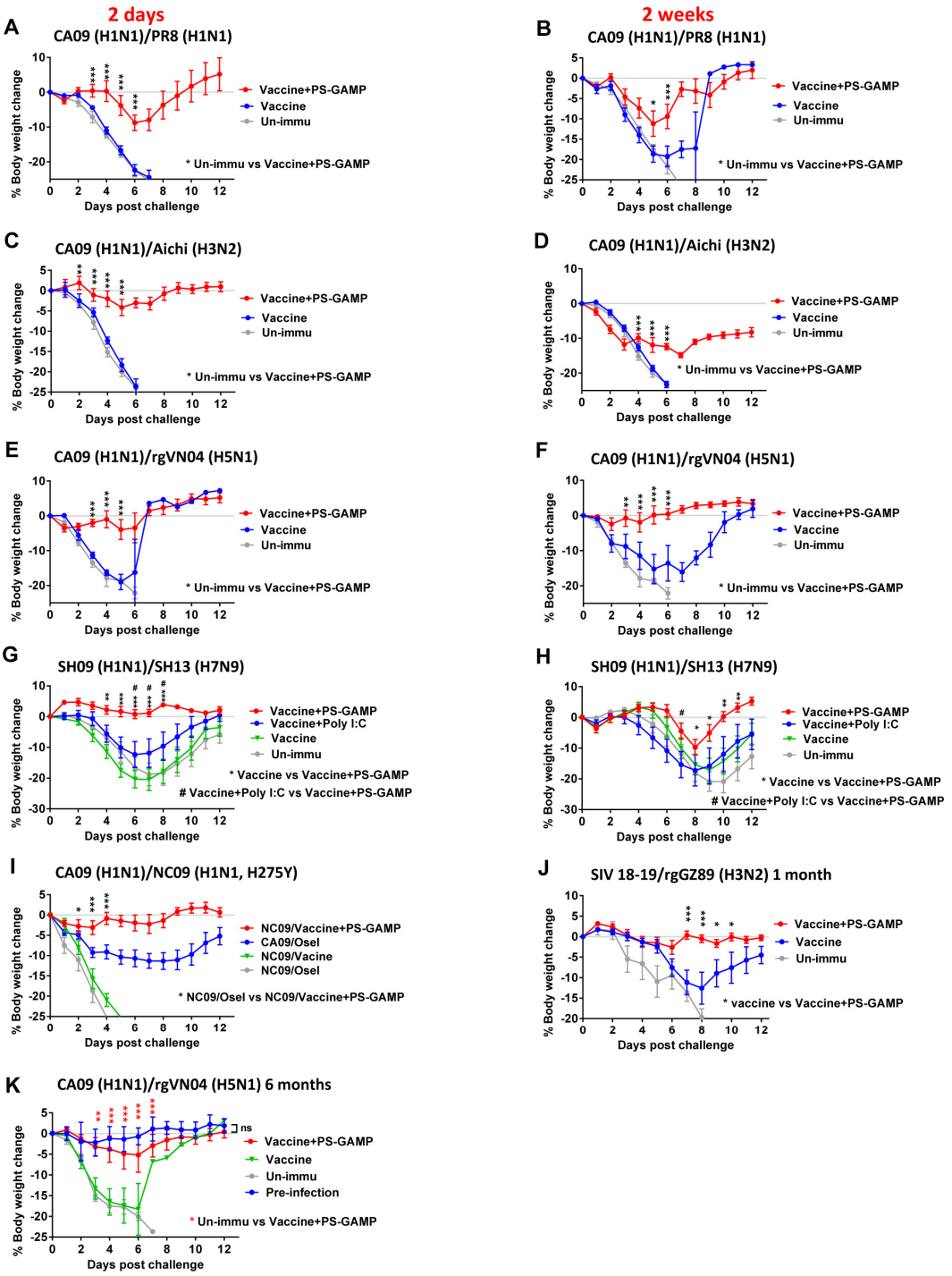

Fig. S27. Supplementary data for cross-protection studies.

(**A** to **K**) Body weight changes corresponding to mice described in **Fig. 6, A to K**, respectively. The results were presented as means ± SEM. Statistical analysis, two-way ANOVA. *p<0.05, **p< 0.01, ***p<0.001, and # p<0.05. All experiments were repeated twice with similar results.

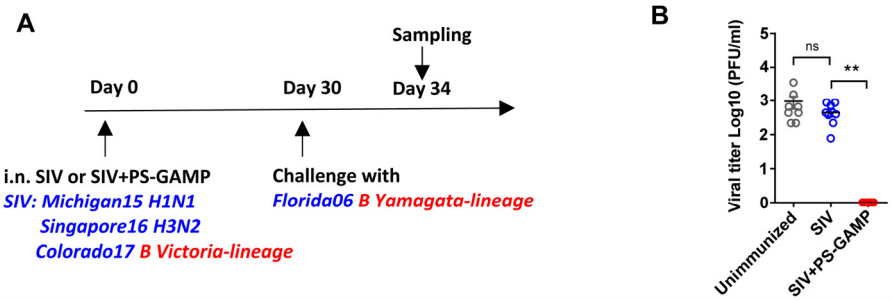

Fig. S28. Vaccination with trivalent seasonal influenza vaccine and PS-GAMP induces cross-protective immunity against mismatched influenza B virus.

(**A**) A schematic of the vaccination/sampling schedule. BALB/c mice were immunized with trivalent seasonal influenza vaccine (2018-19) (SIV) alone or together with 20 μg of PS-GAMP and challenged 1 month later with 4×10^5 $TCID_{50}$ mismatched Florida06 B virus. (**B**) Lungs were isolated 4 d after the immunization and analyzed for viral titers. Each symbol represents individual mice in (**B**). n=8-9. The results were presented as means ± SEM. Statistical analysis, one-way ANOVA. **p<0.01 in the presence or absence of PS-GAMP. ns, no significance. The experiment was repeated twice with similar results.

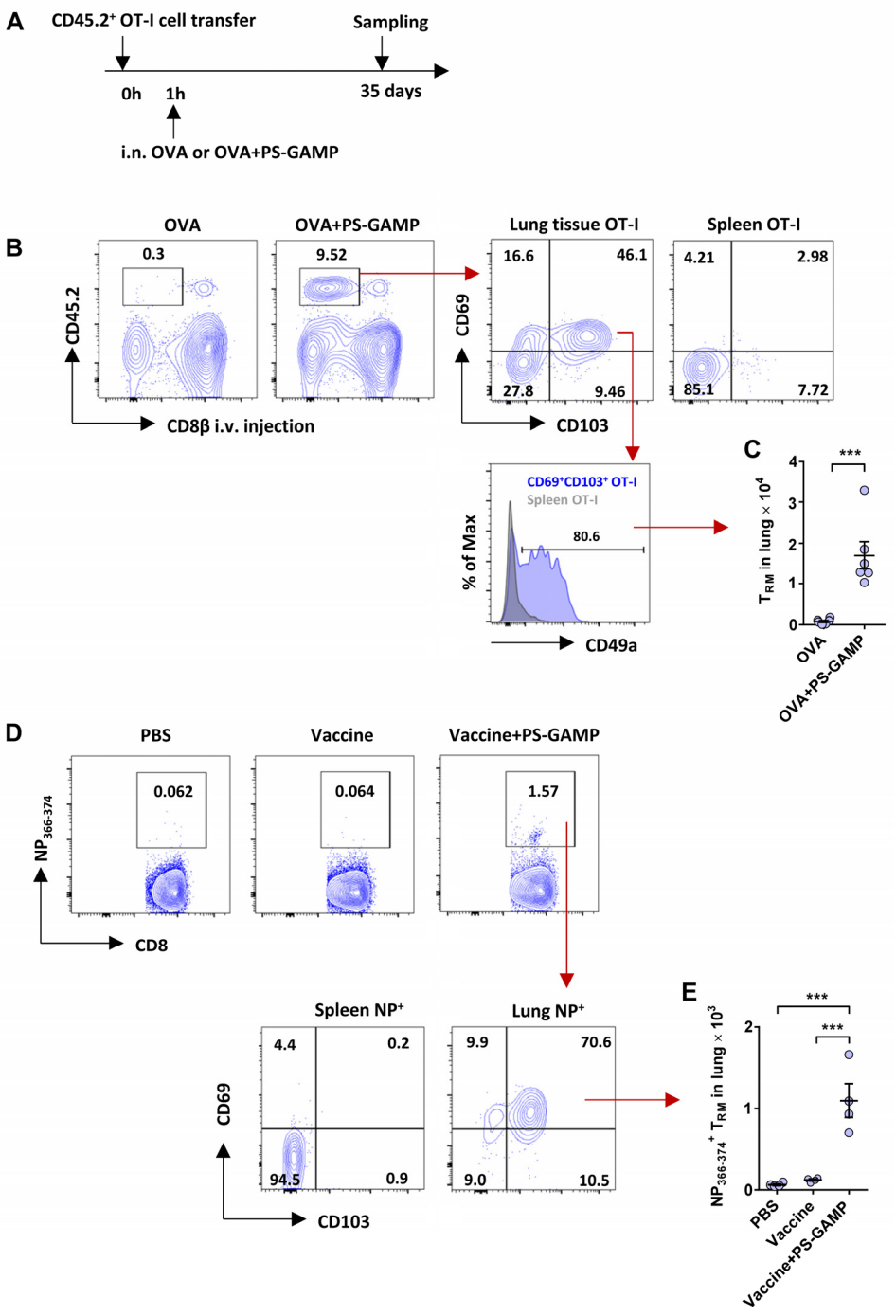

Fig. S29. PS-GAMP/inactivated influenza vaccine induces viral-specific lung CD8$^+$ T_{RM} cells.

(**A**) A schematic of the vaccination/sampling timeline of OT-I mouse model. Mice were transferred with OT-I cells and i.n. immunized 1 h later with OVA in presence or absence of PS-GAMP. Thirty-five d later, mice were i.v. injected with anti-CD8β antibody to exclude circulating CD8$^+$ T cells before sacrificed for flow cytometric analysis. (**B**) Total

$CD8^+$ T cells in the lung were gated by $CD3^+$ and $CD8\alpha^+$ (profile not shown) and lung OT-I cells were recognized as $CD45.2^+$ and $CD8\beta^-$ (antibody i.v. injected) (1^{st} two panels). OT-I cells with T_{RM} phenotype were identified as $CD103^+CD69^+CD49a^+$. OT-I cells in the spleen served as the control (Gray). The number of lung OT-I T_{RM} cells were summarized in (**C**). n=6. (**D** and **E**) Mice were i.n. immunized with CA09 H1N1 vaccine in the presence or absence of PS-GAMP. Lungs were isolated 6 months later for flow cytometry. $NP_{366-374}^+$ $CD8^+$ T cells were gated and validated for CD103 and CD69 expression (**D**) and the number of $NP_{366-374}^+$ $CD8^+$ T_{RM} cells were summarized in (**E**). n=4. $NP_{366-374}^+$ $CD8^+$ T cells in the spleen served as the control. The results were presented as means ± SEM. Statistical analysis, *t*-test for (**C**), one-way ANOVA for (**E**). ***$p<0.001$ in the presence or absence of PS-GAMP. All experiments were repeated twice with similar results.

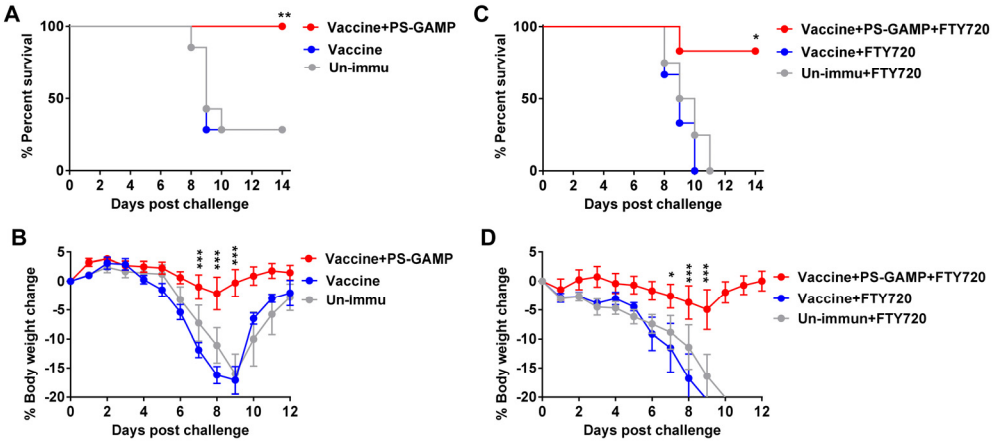

Fig. S30. FTY720 did not affect the cross-protection elicited by influenza vaccine/PS-GAMP.

(**A** and **B**) Mice were i.n. immunized with CA09 H1N1 vaccine alone or together with 20 μg of PS-GAMP and challenged 1 month later with 5×LD_{50} GZ89 H3N2 virus. (**C** and **D**) Mice were immunized and challenged as **A** and **B** except that the mice additionally received daily injections of FTY720 (1 mg/kg/day) from −2 to 14 days after the challenge. n=6-8. Statistical analysis, two-way ANOVA for (**B** and **D**) and Log-rank test for (**A** and **C**). *p<0.05, **p<0.01, and ***p<0.001 compared to the vaccine alone. All experiments were repeated twice with similar results.

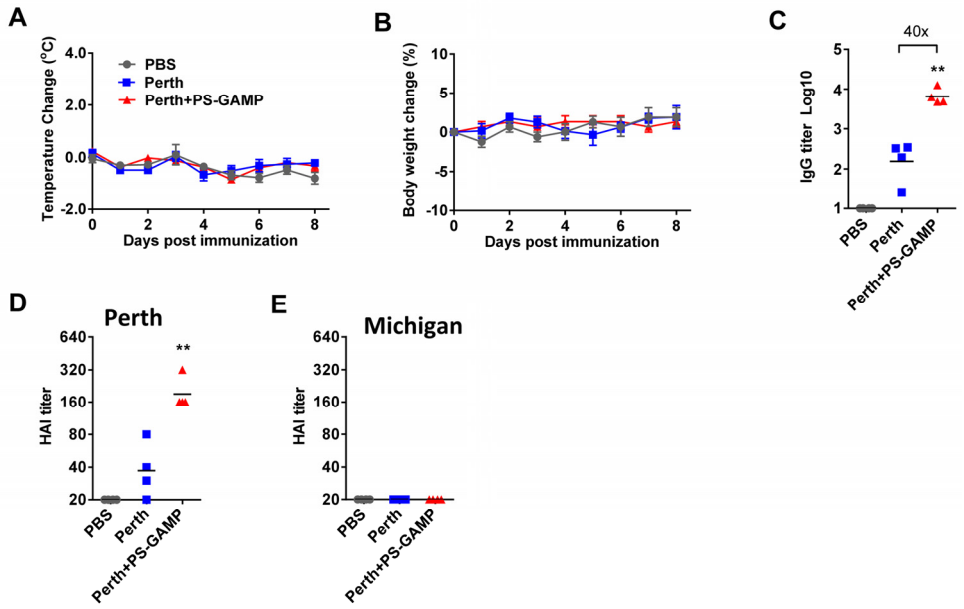

Fig. S31. Safety and efficacy of PS-GAMP in ferrets.

Ferrets were i.n. immunized with an inactivated viral vaccine (Perth H3N2 15 μg) with or without 200 μg of PS-GAMP. Body weight (**A**) and temperature (**B**) of the animals were monitored for 6 d. (**C**) Sera were collected 4 weeks after the immunization and tested for PerthH3N2-specific IgG titers (**C**). HAI titers were also measured against PerthH3N2 (**D**) or MichiganH1N1 (**E**) viral strains. n=4. Each symbol represents individual animals in **C** to **E**. The results were presented as means ± SEM. Statistical analysis, one-way ANOVA for (**C** and **D**). **p< 0.01 compared in the presence vs. absence of PS-GAMP.

Table S1.

Supplementary Table 1. Ferret Clinical Symptom Scores (*44*)

Score	Nasal symptoms	Activity level (playfulness)
0	No symptoms	Fully playful
1	Nasal rattling or sneezing	Responds to play overtures but does not initiate play activity
2	Nasal discharge on external nares	Alert but not playful
3	Mouth breathing	Not playful, not alert

Table S2.

Antibodies and Tetramers for flow cytometry

Antibody	Clone	Label	Vendor	Concentration
$NP_{366-374}$ MHC I tetramers	N/A	AF647	NIH Tetramer Core	7.5 µg/ml
$PA_{224-233}$ MHC I tetramers	N/A	APC	NIH Tetramer Core	7.5 µg/ml
$PB1_{703-711}$ MHC I tetramers	N/A	APC	NIH Tetramer Core	7.5 µg/ml
anti-Ly6G	1A8	APC	Biolegend	2.0 µg/ml
anti-CD11c	N418	AF488	Biolegend	2.5 µg/ml
anti-CD11b	M1/70	BV421	Biolegend	2.0 µg/ml
	M1/70	PerCP/Cy5.5	Biolegend	2.0 µg/ml
	M1/70	PE	Biolegend	2.0 µg/ml
anti-Ly6C	HK1.4	Pacific Blue	Biolegend	5.0 µg/ml
	HK1.4	APC	Biolegend	2.0 µg/ml
anti-CD24	M1/69	Pacific Blue	Biolegend	5.0 µg/ml
anti-EpCAM	G8.8	PerCP/Cy5.5	Biolegend	2.0 µg/ml
	G8.8	PE	Biolegend	1.0 µg/ml
	G8.8	APC	Biolegend	2.0 µg/ml
anti-CD40	3/23	PE	Biolegend	2.0 µg/ml
anti-CD86	GL-1	PerCP/Cy5.5	Biolegend	1.0 µg/ml
anti-CD8α	53-6.7	PerCP/Cy5.5	Biolegend	1.0 µg/ml
	53-6.7	APC	Biolegend	1.0 µg/ml
	53-6.7	PE	Biolegend	2.5 µg/ml
	53-6.7	AF488	Biolegend	5.0 µg/ml
	53-6.7	APC/Cy7	Biolegend	4.0 µg/ml
anti-CD8β	53-5.8	PE/Cy7	Biolegend	2.0 µg/ml
	H35-7.2	PE/Cy7	eBioscience	4.0 µg/ml
anti-CD3	17A2	PE	Biolegend	2.0 µg/ml
	500A2	AF647	eBioscience	1.0 µg/ml
	145-2C11	APC/Cy7	Biolegend	2.0 µg/ml
	17A2	APC/Cy7	Biolegend	4.0 µg/ml
	500A2	FITC	Biolegend	5.0 µg/ml
anti-Granzyme B	GB11	AF647	Biolegend	1 test
	GB11	Pacific Blue	Biolegend	1 test
anti-CD4	GK1.5	APC/Cy7	Biolegend	5.0 µg/ml
	GK1.5	FITC	Biolegend	5.0 µg/ml
	GK1.5	Pacific Blue	Biolegend	5.0 µg/ml
anti-IFNγ	XMG1.2	BV421	Biolegend	1.0 µg/ml
anti-MHC II	M5/114.15.2	APC/Fire750	Biolegend	4.0 µg/ml
anti-Siglec F	S17007L	APC	Biolegend	2.0 µg/ml
anti-CD103	2E7	PE/Cy7	Biolegend	5.0 µg/ml
	2E7	BV421	Biolegend	4.0 µg/ml
anti-CD69	H1.2F3	BV510	Biolegend	2.0 µg/ml
anti-CD49a	HMα1	PE	Biolegend	4.0 µg/ml

anti-NK1.1	PK136	PE	Biolegend	2.0 µg/ml
anti-CD45.1	A20	PE	Biolegend	2.0 µg/ml
anti-CD45.2	104	AF647	Biolegend	2.5 µg/ml

Table S3.

Supplementary Table 3. Primers for Real-time PCR

Gene	Forward 5'-3'	Reverse 5'-3'
Gapdh	ATCAAGAAGGTGGTGAAGCA	AGACAACCTGGTCCTCAGTGT
Ifnb1	AGCTCCAAGAAAGGACGAACA	GCCCTGTAGGTGAGGTTGAT
Tnf	CCTGTAGCCCACGTCGTAG	GGGAGTAGACAAGGTACAACCC
Il10	GCTGGACAACATACTGCTAACC	ATTTCCGATAAGGCTTGGCAA
Cxcl10	CCAAGTGCTGCCGTCATTTTC	TCCCTATGGCCCTCATTCTCA
Ccl2	TCTGGGCCTGCTGTTCACA	CCTACTCATTGGGATCATCTTGCT
Ccl3	TGTACCATGACACTCTGCAAC	CAACGATGAATTGGCGTGGAA
Ccl5	GCCCACGTCAAGGAGTATTTCTA	ACACACTTGGCGGTTCCTTC
Gmcsf	GAAGCATGTAGAGGCCATCA	GAATATCTTCAGGCGGGTCT

References and Notes

1. C. I. Paules, S. G. Sullivan, K. Subbarao, A. S. Fauci, Chasing seasonal influenza—The need for a universal influenza vaccine. *N. Engl. J. Med.* **378**, 7–9 (2018). doi:10.1056/NEJMp1714916 Medline

2. A. Pizzolla, T. H. O. Nguyen, S. Sant, J. Jaffar, T. Loudovaris, S. I. Mannering, P. G. Thomas, G. P. Westall, K. Kedzierska, L. M. Wakim, Influenza-specific lung-resident memory T cells are proliferative and polyfunctional and maintain diverse TCR profiles. *J. Clin. Invest.* **128**, 721–733 (2018). doi:10.1172/JCI96957 Medline

3. K. D. Zens, J. K. Chen, D. L. Farber, Vaccine-generated lung tissue-resident memory T cells provide heterosubtypic protection to influenza infection. *JCI Insight* **1**, 85832 (2016). doi:10.1172/jci.insight.85832 Medline

4. S. Sridhar, S. Begom, A. Bermingham, K. Hoschler, W. Adamson, W. Carman, T. Bean, W. Barclay, J. J. Deeks, A. Lalvani, Cellular immune correlates of protection against symptomatic pandemic influenza. *Nat. Med.* **19**, 1305–1312 (2013). doi:10.1038/nm.3350 Medline

5. J. T. Weinfurter, K. Brunner, S. V. Capuano 3rd, C. Li, K. W. Broman, Y. Kawaoka, T. C. Friedrich, Cross-reactive T cells are involved in rapid clearance of 2009 pandemic H1N1 influenza virus in nonhuman primates. *PLOS Pathog.* **7**, e1002381 (2011). doi:10.1371/journal.ppat.1002381 Medline

6. M. Koutsakos, P. T. Illing, T. H. O. Nguyen, N. A. Mifsud, J. C. Crawford, S. Rizzetto, A. A. Eltahla, E. B. Clemens, S. Sant, B. Y. Chua, C. Y. Wong, E. K. Allen, D. Teng, P. Dash, D. F. Boyd, L. Grzelak, W. Zeng, A. C. Hurt, I. Barr, S. Rockman, D. C. Jackson, T. C. Kotsimbos, A. C. Cheng, M. Richards, G. P. Westall, T. Loudovaris, S. I. Mannering, M. Elliott, S. G. Tangye, L. M. Wakim, J. Rossjohn, D. Vijaykrishna, F. Luciani, P. G. Thomas, S. Gras, A. W. Purcell, K. Kedzierska, Human $CD8^+$ T cell cross-reactivity across influenza A, B and C viruses. *Nat. Immunol.* **20**, 613–625 (2019). doi:10.1038/s41590-019-0320-6 Medline

7. L. Si, H. Xu, X. Zhou, Z. Zhang, Z. Tian, Y. Wang, Y. Wu, B. Zhang, Z. Niu, C. Zhang, G. Fu, S. Xiao, Q. Xia, L. Zhang, D. Zhou, Generation of influenza A viruses as live but replication-incompetent virus vaccines. *Science* **354**, 1170–1173 (2016). doi:10.1126/science.aah5869 Medline

8. L. Wang, S.-Y. Liu, H.-W. Chen, J. Xu, M. Chapon, T. Zhang, F. Zhou, Y. E. Wang, N. Quanquin, G. Wang, X. Tian, Z. He, L. Liu, W. Yu, D. J. Sanchez, Y. Liang, T. Jiang, R. Modlin, B. R. Bloom, Q. Li, J. C. Deng, P. Zhou, F. X.-F. Qin, G. Cheng, Generation of a live attenuated influenza vaccine that elicits broad protection in mice and ferrets. *Cell Host Microbe* **21**, 334–343 (2017). doi:10.1016/j.chom.2017.02.007 Medline

9. D. F. Hoft, E. Babusis, S. Worku, C. T. Spencer, K. Lottenbach, S. M. Truscott, G. Abate, I. G. Sakala, K. M. Edwards, C. B. Creech, M. A. Gerber, D. I. Bernstein, F. Newman, I. Graham, E. L. Anderson, R. B. Belshe, Live and inactivated influenza vaccines induce similar humoral responses, but only live vaccines induce diverse T-cell responses in young children. *J. Infect. Dis.* **204**, 845–853 (2011). doi:10.1093/infdis/jir436 Medline

10. A. Ablasser, M. Goldeck, T. Cavlar, T. Deimling, G. Witte, I. Röhl, K.-P. Hopfner, J. Ludwig, V. Hornung, cGAS produces a 2′-5′-linked cyclic dinucleotide second messenger that activates STING. *Nature* **498**, 380–384 (2013). doi:10.1038/nature12306 Medline

11. J. Wu, L. Sun, X. Chen, F. Du, H. Shi, C. Chen, Z. J. Chen, Cyclic GMP-AMP is an endogenous second messenger in innate immune signaling by cytosolic DNA. *Science* **339**, 826–830 (2013). doi:10.1126/science.1229963 Medline

12. X. D. Li, J. Wu, D. Gao, H. Wang, L. Sun, Z. J. Chen, Pivotal roles of cGAS-cGAMP signaling in antiviral defense and immune adjuvant effects. *Science* **341**, 1390–1394 (2013). doi:10.1126/science.1244040 Medline

13. J. Wang, P. Li, M. X. Wu, Natural STING Agonist as an “Ideal” adjuvant for cutaneous vaccination. *J. Invest. Dermatol.* **136**, 2183–2191 (2016). doi:10.1016/j.jid.2016.05.105 Medline

14. L. Corrales, L. H. Glickman, S. M. McWhirter, D. B. Kanne, K. E. Sivick, G. E. Katibah, S.-R. Woo, E. Lemmens, T. Banda, J. J. Leong, K. Metchette, T. W. Dubensky Jr., T. F. Gajewski, Direct activation of STING in the tumor microenvironment leads to potent and systemic tumor regression and immunity. *Cell Reports* **11**, 1018–1030 (2015). doi:10.1016/j.celrep.2015.04.031 Medline

15. J. A. Whitsett, S. E. Wert, T. E. Weaver, Alveolar surfactant homeostasis and the pathogenesis of pulmonary disease. *Annu. Rev. Med.* **61**, 105–119 (2010). doi:10.1146/annurev.med.60.041807.123500 Medline

16. K. A. Woodrow, K. M. Bennett, D. D. Lo, Mucosal vaccine design and delivery. *Annu. Rev. Biomed. Eng.* **14**, 17–46 (2012). doi:10.1146/annurev-bioeng-071811-150054 Medline

17. E. Parra, J. Pérez-Gil, Composition, structure and mechanical properties define performance of pulmonary surfactant membranes and films. *Chem. Phys. Lipids* **185**, 153–175 (2015). doi:10.1016/j.chemphyslip.2014.09.002 Medline

18. A. V. Misharin, L. Morales-Nebreda, G. M. Mutlu, G. R. Budinger, H. Perlman, Flow cytometric analysis of macrophages and dendritic cell subsets in the mouse lung. *Am. J. Respir. Cell Mol. Biol.* **49**, 503–510 (2013). doi:10.1165/rcmb.2013-0086MA Medline

19. H. Qin, C. A. Wilson, S. J. Lee, X. Zhao, E. N. Benveniste, LPS induces CD40 gene expression through the activation of NF-κB and STAT-1α in macrophages and microglia. *Blood* **106**, 3114–3122 (2005). doi:10.1182/blood-2005-02-0759 Medline

20. A. Haczku, Protective role of the lung collectins surfactant protein A and surfactant protein D in airway inflammation. *J. Allergy Clin. Immunol.* **122**, 861–881 (2008). doi:10.1016/j.jaci.2008.10.014 Medline

21. J. Wang, B. Li, M. X. Wu, Effective and lesion-free cutaneous influenza vaccination. *Proc. Natl. Acad. Sci. U.S.A.* **112**, 5005–5010 (2015). doi:10.1073/pnas.1500408112 Medline

22. J. Wang, D. Shah, X. Chen, R. R. Anderson, M. X. Wu, A micro-sterile inflammation array as an adjuvant for influenza vaccines. *Nat. Commun.* **5**, 4447 (2014). doi:10.1038/ncomms5447 Medline

23. A. Ballesteros-Tato, B. León, F. E. Lund, T. D. Randall, Temporal changes in dendritic cell subsets, cross-priming and costimulation via CD70 control $CD8^+$ T cell responses to influenza. *Nat. Immunol.* **11**, 216–224 (2010). doi:10.1038/ni.1838 Medline

24. B. Unkel, K. Hoegner, B. E. Clausen, P. Lewe-Schlosser, J. Bodner, S. Gattenloehner, H. Janßen, W. Seeger, J. Lohmeyer, S. Herold, Alveolar epithelial cells orchestrate DC function in murine viral pneumonia. *J. Clin. Invest.* **122**, 3652–3664 (2012). doi:10.1172/JCI62139 Medline

25. J. S. Sullivan, P. W. Selleck, T. Downton, I. Boehm, A. M. Axell, Y. Ayob, N. M. Kapitza, W. Dyer, A. Fitzgerald, B. Walsh, G. W. Lynch, Heterosubtypic anti-avian H5N1 influenza antibodies in intravenous immunoglobulins from globally separate populations protect against H5N1 infection in cell culture. *J. Mol. Genet. Med.* **3**, 217–224 (2009). Medline

26. C. W. Lawrence, R. M. Ream, T. J. Braciale, Frequency, specificity, and sites of expansion of $CD8^+$ T cells during primary pulmonary influenza virus infection. *J. Immunol.* **174**, 5332–5340 (2005). doi:10.4049/jimmunol.174.9.5332 Medline

27. T. Ichinohe, I. Watanabe, S. Ito, H. Fujii, M. Moriyama, S. Tamura, H. Takahashi, H. Sawa, J. Chiba, T. Kurata, T. Sata, H. Hasegawa, Synthetic double-stranded RNA poly(I:C) combined with mucosal vaccine protects against influenza virus infection. *J. Virol.* **79**, 2910–2919 (2005). doi:10.1128/JVI.79.5.2910-2919.2005 Medline

28. J. Y. Kang, X. Nan, M. S. Jin, S.-J. Youn, Y. H. Ryu, S. Mah, S. H. Han, H. Lee, S.-G. Paik, J.-O. Lee, Recognition of lipopeptide patterns by Toll-like receptor 2-Toll-like receptor 6 heterodimer. *Immunity* **31**, 873–884 (2009). doi:10.1016/j.immuni.2009.09.018 Medline

29. A. Ablasser, J. L. Schmid-Burgk, I. Hemmerling, G. L. Horvath, T. Schmidt, E. Latz, V. Hornung, Cell intrinsic immunity spreads to bystander cells via the intercellular transfer of cGAMP. *Nature* **503**, 530–534 (2013). doi:10.1038/nature12640 Medline

30. K. Westphalen, G. A. Gusarova, M. N. Islam, M. Subramanian, T. S. Cohen, A. S. Prince, J. Bhattacharya, Sessile alveolar macrophages communicate with alveolar epithelium to modulate immunity. *Nature* **506**, 503–506 (2014). doi:10.1038/nature12902 Medline

31. P. W. Furlow, S. Zhang, T. D. Soong, N. Halberg, H. Goodarzi, C. Mangrum, Y. G. Wu, O. Elemento, S. F. Tavazoie, Mechanosensitive pannexin-1 channels mediate microvascular metastatic cell survival. *Nat. Cell Biol.* **17**, 943–952 (2015). doi:10.1038/ncb3194 Medline

32. Q. Chen, A. Boire, X. Jin, M. Valiente, E. E. Er, A. Lopez-Soto, L. Jacob, R. Patwa, H. Shah, K. Xu, J. R. Cross, J. Massagué, Carcinoma-astrocyte gap junctions promote brain metastasis by cGAMP transfer. *Nature* **533**, 493–498 (2016). doi:10.1038/nature18268 Medline

33. H. Ramsey, Q. Zhang, D. E. Brown, D. P. Steensma, C. P. Lin, M. X. Wu, Stress-induced hematopoietic failure in the absence of immediate early response gene X-1 (IEX-1, IER3). *Haematologica* **99**, 282–291 (2014). doi:10.3324/haematol.2013.092452 Medline

34. J. H. Fritz, L. Le Bourhis, J. G. Magalhaes, D. J. Philpott, Innate immune recognition at the epithelial barrier drives adaptive immunity: APCs take the back seat. *Trends Immunol.* **29**, 41–49 (2008). doi:10.1016/j.it.2007.10.002 Medline

35. S. A. Saenz, B. C. Taylor, D. Artis, Welcome to the neighborhood: Epithelial cell-derived cytokines license innate and adaptive immune responses at mucosal sites. *Immunol. Rev.* **226**, 172–190 (2008). doi:10.1111/j.1600-065X.2008.00713.x Medline

36. J. A. Whitsett, T. Alenghat, Respiratory epithelial cells orchestrate pulmonary innate immunity. *Nat. Immunol.* **16**, 27–35 (2015). doi:10.1038/ni.3045 Medline

37. R. Hai, M. Schmolke, V. H. Leyva-Grado, R. R. Thangavel, I. Margine, E. L. Jaffe, F. Krammer, A. Solórzano, A. García-Sastre, P. Palese, N. M. Bouvier, Influenza A(H7N9) virus gains neuraminidase inhibitor resistance without loss of in vivo virulence or transmissibility. *Nat. Commun.* **4**, 2854 (2013). doi:10.1038/ncomms3854 Medline

38. C. Moore, M. Galiano, A. Lackenby, T. Abdelrahman, R. Barnes, M. R. Evans, C. Fegan, S. Froude, M. Hastings, S. Knapper, E. Litt, N. Price, R. Salmon, M. Temple, E. Davies, Evidence of person-to-person transmission of oseltamivir-resistant pandemic influenza A(H1N1) 2009 virus in a hematology unit. *J. Infect. Dis.* **203**, 18–24 (2011). doi:10.1093/infdis/jiq007 Medline

39. A. Hidalgo, A. Cruz, J. Pérez-Gil, Barrier or carrier? Pulmonary surfactant and drug delivery. *Eur. J. Pharm. Biopharm.* **95** (Pt A), 117–127 (2015). doi:10.1016/j.ejpb.2015.02.014 Medline

40. B. Olsson *et al*., in *Controlled Pulmonary Drug Delivery*, A. J. H. Hugh D.C. Smyth, Ed. (Springer-Verlag, 2011), pp. 21–50.

41. J. C. Sung, B. L. Pulliam, D. A. Edwards, Nanoparticles for drug delivery to the lungs. *Trends Biotechnol.* **25**, 563–570 (2007). doi:10.1016/j.tibtech.2007.09.005 Medline

42. I. J. Bakken, K. M. Aaberg, S. Ghaderi, N. Gunnes, L. Trogstad, P. Magnus, S. E. Håberg, Febrile seizures after 2009 influenza A (H1N1) vaccination and infection: A nationwide registry-based study. *BMC Infect. Dis.* **15**, 506 (2015). doi:10.1186/s12879-015-1263-7 Medline

43. F. Szoka Jr., D. Papahadjopoulos, Procedure for preparation of liposomes with large internal aqueous space and high capture by reverse-phase evaporation. *Proc. Natl. Acad. Sci. U.S.A.* **75**, 4194–4198 (1978). doi:10.1073/pnas.75.9.4194 Medline

44. Y. Matsuoka, E. W. Lamirande, K. Subbarao, The ferret model for influenza. *Curr. Protoc. Microbiol.* **13**, 15G.2.1–15G.2.29 (2009).

45. J. Wang, H.-J. Chen, T. Hang, Y. Yu, G. Liu, G. He, S. Xiao, B. R. Yang, C. Yang, F. Liu, J. Tao, M. X. Wu, X. Xie, Physical activation of innate immunity by spiky particles. *Nat. Nanotechnol.* **13**, 1078–1086 (2018). doi:10.1038/s41565-018-0274-0 Medline

46. C. L. Schengrund, X. Chi, J. Sabol, J. W. Griffith, Long-term effects of instilled mineral dusts on pulmonary surfactant isolated from monkeys. *Lung* **173**, 197–208 (1995). doi:10.1007/BF00175660 Medline

47. L. Wang, M. P. Pileni, Encapsulation of zwitterionic Au nanocrystals into liposomes by reverse phase evaporation method: Influence of the surface charge. *Langmuir* **32**, 12370–12377 (2016). doi:10.1021/acs.langmuir.6b01132 Medline

48. A. V. Li, J. J. Moon, W. Abraham, H. Suh, J. Elkhader, M. A. Seidman, M. Yen, E.-J. Im, M. H. Foley, D. H. Barouch, D. J. Irvine, Generation of effector memory T cell-based

mucosal and systemic immunity with pulmonary nanoparticle vaccination. *Sci. Transl. Med.* **5**, 204ra130 (2013). doi:10.1126/scitranslmed.3006516 Medline

49. G. Matute-Bello, G. Downey, B. B. Moore, S. D. Groshong, M. A. Matthay, A. S. Slutsky, W. M. Kuebler; Acute Lung Injury in Animals Study Group, An official American Thoracic Society workshop report: Features and measurements of experimental acute lung injury in animals. *Am. J. Respir. Cell Mol. Biol.* **44**, 725–738 (2011). doi:10.1165/rcmb.2009-0210ST Medline